# Icosahedral quasicrystal decoration models. II. Optimization under realistic Al-Mn potentials

M. Mihalkovič*
*Department of Physics, Cornell University, Ithaca, New York 14853-2501*
*and Laboratoire de Thermodynamique et Physique-Chimie Métallurgiques, Ecole Nationale Supérieure d'Electronique et d'Electromécanique de Grenoble, Boîte Postale 75, 38402 St. Martin d'Heres Cedex, France*

W.-J. Zhu and C. L. Henley
*Department of Physics, Cornell University, Ithaca, New York 14853-2501*

R. Phillips
*Division of Engineering, Brown University, Providence, Rhode Island 02912*
(Received 26 June 1995; revised manuscript received 26 December 1995)

We have constructed and relaxed over 200 different finite structure models for the quasicrystal *i*-AlMn based on decorations of the ''canonical-cell tiling.'' We adopted *ab initio*-based pair potentials with strong Friedel oscillations, which reproduce the phase diagram of real Al-Mn intermetallic crystal structures fairly well. Our various decoration rules encompass cases with face-centered icosahedral (FCI) symmetry and with simple icosahedral (SI) symmetry, and include additional variations in the occupancy and/or chemistry of certain site types. Each decoration was applied to 11 distinct periodic approximants of the tiling. We found that (i) the relaxed atomic positions of each site type can be closely approximated by fixed positions on each tile type, even though the environments (beyond the first neighbor) are inequivalent. (ii) Models with simple icosahedral (SI) space-group symmetry were better than those with face-centered icosahedral (FCI) space-group symmetry. (iii) ''Loose'' decorations, containing voids almost large enough for an atom, were better than the ''dense'' decorations which were suggested by packing considerations. (iv) Our results depended on using the realistic potentials; *short*-range potentials favor the ''dense'' structures, and many details depend on the second or further oscillations in the potentials. (v) For our best model, there is relatively little variation of the energy when tiles are rearranged, i.e., a *random-tiling model* is a good zero-order description of the system.

## I. INTRODUCTION

Quasicrystals raise at least two interesting questions:

(i) What causes the atoms to adopt these aperiodic, yet ordered structures? How can the quasicrystal structure have a lower free energy than any competing crystalline one for certain compositions, as in *i*-AlPdMn?

(ii) Where do the exotic electronic transport properties come from? Experiments find an extremely high resistivity, which is ascribed to localized states or possibly to ''spiky'' features of the density of states.[1–3]

Answers to both questions require electronic-structure calculations. These are inherently difficult, not only due to the absence of a finite unit cell, but also because the electronic structure of Al-transition metal (Al-TM) alloys is technically difficult to model, owing to the combination of *sp* and *d* bands near the Fermi level. In addition, electronic-structure calculations demand knowledge of the atomic positions, which are nontrivial to describe. A perfect quasiperiodic structure requires (in principle) an infinite number of parameters to specify the positions of its atoms; moreover, if a quasicrystal phase are stabilized by entropy,[4,5] then its structure is intrinsically random.

In a companion paper[6] (henceforth called ''paper I''), we argued that many electronic calculations depend on having a reasonably correct local geometry around *every atom*, a level of perfection which cannot be delivered by structural refinements of diffraction data. We proposed instead a unified approach to quasicrystal structure determination, in which diffraction fitting (guided also by geometric intuition based upon known crystalline approximants) is *combined* with optimization of the total energy — here represented by pair potentials — to discover where the atoms are. In this paper we carry out a prototype of the second part of this program, by exploring the structural energies of a family of atomic models for *i*-AlMn, which is descended from the model of Ref. 7.

Structural models for icosahedral quasicrystals are commonly represented as cuts (at irrational orientations) through densities which are periodic in a six-dimensional (6D) hyperspace. For this paper, however, we adopted the alternate formalism of cluster-based decoration models, based in this case on the canonical-cell tiling (CCT).[8] A decoration model consists of a geometrical framework (most often a tiling), and a set of local rules for decorating this framework with atoms (detailed definitions are found in paper I, Sec. II). We have adopted the decoration approach because

(i) we wished to explore an alternative to the ''six-dimensional'' technology;

(ii) it permits the systematic study of the energy changes due to tile rearrangements;

(iii) this approach appears to be more convenient when we wish to make many variations of the models (as here).

We have studied two general families of decorations which we have called ''dense'' and ''loose.'' This paper concentrates on the ''loose'' family since they turn out to be noticeably superior in energy to the ''dense'' models. The specific models here were presented in detail in paper I as

 

were the general concepts of systematic tile-decoration models which in the present work were found useful for understanding the interplay between potentials, geometry, and the resulting energies (in Secs. IV and II of paper I, respectively.)

All known stable, highly ordered quasicrystals (e.g., *i*-AlPdMn) belong to ternary systems; in this paper, however, we consider only Al-Mn structures. Our reasons for imposing this rather severe restriction are the following:

(i) The parameter space of a binary phase diagram (at $T=0$) can be explored by tuning a single parameter, the manganese concentration $x_{\mathrm{Mn}}$.

(ii) In the Al-Mn system of alloys, we may be guided by the many crystalline phases with solved structures, that are similar in their composition and in their local atomic order to the (metastable) *i*-AlMn phase.

(iii) Realistic pair potentials have not yet, to our knowledge, been computed for any Al-transition-metal ternary system.

The paper is organized as follows. In Sec. II, we describe in detail the pair potentials used in this study — the first of the two essential inputs to our calculation. In particular, we comment on the derivation of the potentials and provide a critical analysis of their expected virtues and drawbacks. This is followed by a sketch of the coupling between geometrical motifs and the shape and character of the potentials as well as a description of the techniques we have used to carry out structural relaxations. In Sec. III, we test the validity of pair potentials as a tool for structural discrimination by applying them to a variety of real and hypothetical crystalline structures in the Al-Mn system indeed, we obtain a mostly correct picture of the Al-Mn (zero-temperature) phase diagram around the quasicrystal forming compositions. Section IV summarizes the models used, the second of the two essential inputs for this work. We also outline the diagnostic criteria which helped us to systematically identify and repair ''problem sites'' in the decoration so as to improve the total energy. (This was one of several technical objectives of the present work, which is intended as a ''prototype'' for future studies.)

The prime objective of our study was to determine which of the families we studied (including ''dense'' FCI, ''dense'' SI, and ''loose'' SI models) had the optimal energy, and to ascertain how significant the long-range interatomic interactions are. Thus the heart of the paper is Sec. V, which reports the results of our systematic comparison of various competing models, which differ in their symmetry (FCI vs SI) and in the tightness of their packing (dense vs loose). In this section we also accomplish a technical objective, by verifying that a decoration model can accurately model the true, relaxed positions of all atoms using a moderate number of real parameters. Section VI provides a brief summary of our parallel work on relaxing models defined within the 6D-cut framework. Section VII presents further tests of the stability of our models and its origins — mostly, it consists of explorations of additional ways in which potentials can be varied. Section VIII gathers the insights of previous sections and attempts to justify our observation that loose structures with SI symmetry are favored. Our total experience shows that it is essential to have the correct potentials and the correct model; the second well of the oscillating potentials is quite significant in selecting among structures.

A final objective of this project was to initiate the study of ''tile Hamiltonian'' (Sec. IX), a reduced Hamiltonian defined in terms of the tile degrees of freedom; calculating this is the bridge from the microscopic to the macroscopic level. Our preliminary results on the tile Hamiltonian support the validity of a random tiling as the zeroth-order description, since different arrangement of tiles have almost the same energies. The conclusions (Sec. X) recapitulate the most important results and outline promising directions for extending or improving our calculation.

There are some precedents for our approach. Some years ago, Lançon and Billard[9] studied the stability of the Duneau-Oguey model[10] for *i*-AlMn(Si), and two variants thereof, under the influence of Morse pair potentials; similar relaxations were carried out by Roth *et al.*[11] for *i*-AlZnMg (in the *i*-AlCuLi family). Our present work differs from theirs in that we used realistic, microscopically derived pair potentials, with no free parameters; that was previously done (in the *i*-AlCuLi rather than the *i*-AlMn family) by Krajči and Hafner,[12] but they did not vary the models. A precursor of the present calculation[13] incorporated a computational scheme which admitted variations, but did not actually pursue them.[13] Widom, Phillips, and collaborators have made investigations similar in spirit to ours for decagonal quasicrystals in the Al-Co system,[14,15] with some variations of different models. However, no previous work has studied a collection of models nearly as extensive as reported here.

## II. PAIR POTENTIALS

Present computational resources allow for *ab initio* calculations only for systems of up to about 500 atoms.[16] Since we relax structures with $4\times10^4$ atoms, we approximate the structural energy by a sum of interatomic potentials,

$$E_{\mathrm{coh}}=\frac{1}{2}\sum_{ij} V_{ij}(r_{ij}), \tag{1}$$

where $r_{ij}$ is the distance between atoms $i$ and $j$. The shape of the potential $V_{ij}(R)$ depends only on the species $i$ and $j$.

If our quasicrystals were alloys of simple metals (such as Al) with $sp$ orbitals, these potentials could be derived from a nearly-free-electron picture based upon pseudopotentials. This approach has been applied to the *i*-AlCuLi family of quasicrystals.[12,17]

On the other hand, if our quasicrystals included only transition metals, the binding would be dominated by $d$ orbitals and could be approached from a tight-binding approximation. This approach was applied to quasicrystals of the *i*-TiMn family.[18] But Al-transition-metal alloys, the case we are studying, present technical difficulties since both tightly bound $d$ bands and also free-electron-like $sp$ bands are present.

### A. Construction of pair potentials

We use effective pair potentials that have been developed for Al-rich AlMn compounds, using a combined pseudopotential and Green's-function method for the Mn-Mn and Al-Mn potentials, and conventional pseudopotential-based perturbation theory for Al-Al pairs. (Details of the construc-

tion may be found in Ref. 19; see also Refs. 20 and 21. The analogous potentials for Al-Co compounds are described in Ref. 14.) We will call our potentials ''realistically oscillating'' because their outstanding feature is the strong Friedel oscillations and, furthermore, the wavelength and magnitudes of the oscillations are calculated using microscopically based approximations.[22]

Such potentials depend parametrically on the density of conduction electrons, which is given simply by

$$\rho_{\rm el}=n_{\rm at}[v_{\rm Al}-(v_{\rm Al}-v_{\rm Mn})x_{\rm Mn}]. \tag{2}$$

The valences (number of electrons contributed to the conduction band) are

$$v_{\rm Al}=3, \quad v_{\rm Mn}=1.5 \tag{3}$$

for Al and Mn, respectively. Equation (2) may be used to compute $\rho_{\rm el}$ for the various structures we studied from the values of $n_{\rm at}$ and $x_{\rm Mn}$ given in our tables. The value $v_{\rm Mn}=1.5$ comes from augmented-spherical-wave (ASW) calculations[23] on an ordered fcc solid solution $Al_3Mn$ in which the number of $d$ electrons per Mn was determined to be 5.5, leaving 7–5.5 = 1.5 free electrons per Mn.

Note that we do *not* adopt the effective *negative* $v_{\rm Mn}$ which was hypothesized on empirical grounds during the 1950's, (in the context of a Hume-Rothery picture). It would be hard to credit a real charge transfer of such a magnitude, but there is theoretical support for negative valence behavior *without* a large shift in $d$ electron number.[24,25] References 24 and 25 present different scenarios: the former says that $k_F$ should be calculated using the usual (positive) valences, but the latter implies that $v_{\rm Mn}\approx -1$ ought to be used.[26]

For this work, we always use potentials calculated for the particular reference density of conduction electrons[27]

$$\rho_0\equiv 0.17792 \ \text{Å}^{-3}. \tag{4}$$

The Al-Al potential (see Fig. 1) has only a shallow and rather narrow minimum at 2.8 Å, and then a deep and broad *second*-neighbor well at about 4.4 Å,[17] whereas the Mn-Mn potential has a strong second-neighbor well at 4.7 Å. These pair potentials also show quite large Friedel oscillations, especially in the Mn-Mn potential. The asymptotic form of Friedel oscillations (neglecting effects of disorder) is

$$V(r)\propto \cos(2k_F r+\phi)/r^3, \tag{5}$$

where $\phi$ is some phase angle.

Thus, pair interactions between second, third, or fourth neighbors might determine the atomic structure. The Friedel oscillations are the equivalent in real space of the ''Hume-Rothery/Jones'' phenomenon in Fourier space, which is believed to be important for stabilizing the icosahedral phase and in producing a pseudogap in the electronic density of states.[1,24] It has even been suggested[2] that such oscillating, long-range potentials might suffice to force a *quasiperiodic* ground state, without the need for local matching rules.

### B. Drawbacks of pair potentials

We would not expect *a priori* that our pair potentials will account for the relative cohesive energy of various structures with enough precision to predict which ones are stable in the real system. The reasons for these doubts are listed below. (An even more detailed discussion of some of these difficulties is found in Ref. 14.) But in fact, as we shall see below (Sec. III), our potentials give a reasonable account of the Al-Mn phase diagram, as long as $x_{\rm Mn}$ is not too far from 0.20 (as in a typical quasicrystal composition) and $\rho_{\rm el}$ is close to $\rho_0$. Therefore, we believe it is plausible that they also give correct answers for many details of the $i$-AlMn structure.

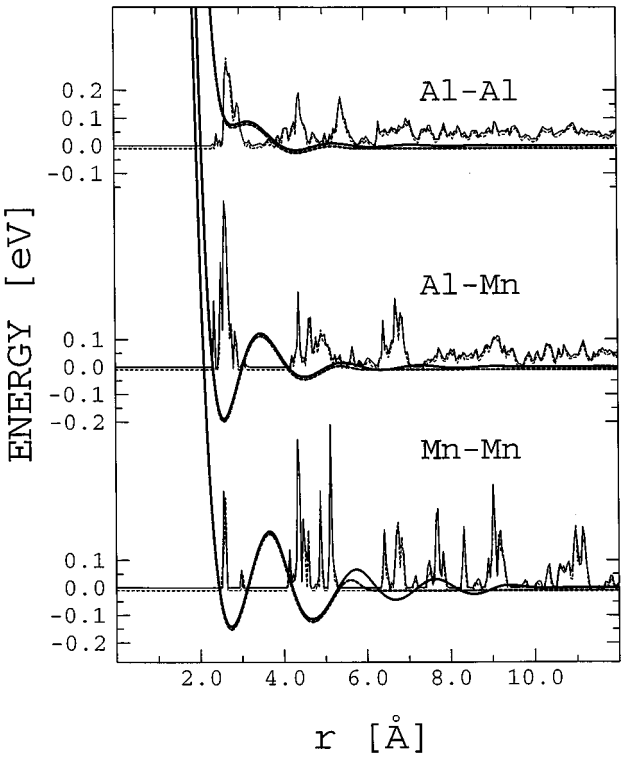


FIG. 1. The three pair potentials for (a) Al-Al, (b) Al-Mn, and (c) Mn-Mn atoms. With each potential is shown the pair-distribution function for the corresponding types of pairs, for the ''loose'' CCT decoration LS1.2 (in the 5/3 approximant tiling $T8$). The solid (dashed) line shows the results using truncation 11 Å (6.2 Å). Note the good match between the peaks of the PDF and the small wells from the Friedel oscillations.

#### 1. Electron density

The forms of the potentials, and in particular the radii at which they have wells, depend upon the conduction-electron density $\rho_{\rm el}$. (The most obvious reason is that the wavelength of Friedel oscillations is $1/2k_F$.) This is worrisome since (as noted above) our potentials should be valid only for the conduction-electron density $\rho_{\rm el}=\rho_0$, but we use them in structures which may have $\rho_{\rm el}\neq\rho_0$.

Of course, the value of $\rho_{\rm el}$ also depends on the quasilattice constant $a_q$. In the present work, unless otherwise noted, the unit cell dimensions were chosen so that $a_q=4.60$ Å as observed experimentally in $i$-AlMnSi.[28] It would have been more precise to adopt instead the experimental value for $i$-AlMn, which is $a_q\sim 4.65$ Å.[29] Had we done so, we would also avoid the concern about using $\rho_{\rm el}\neq\rho_0$, for in fact $\rho_{\rm el}=\rho_0$ would be reproduced by $a_q\approx 4.64$ Å for a typical loose model, or $a_q\approx 4.67$ Å for the densest of the dense

models, close to the observed value in *i*-AlMn.

In any case, for the lattice constants we use and the AlMn compositions of interest to us, $\rho_{\rm el}$ lies within $\sim 2\%$ of $\rho_0$. Since the $\rho_{\rm el}$ values are uncertain anyhow by a comparable amount (due to the $\sim \pm 0.1$ uncertainty in $v_{\rm Mn}$), we feel this is not a serious problem.

#### *2. Structure-independent terms*

A further, more fundamental deficiency in our total energies is that they actually include only the structure-dependent terms; we omit the much larger contributions to the cohesive energy (call their sum $U_0$) which depend (through the jellium total energy, a function of the electron density, and the pseudopotential core radius) on the density and stoichiometry of the cores, but *not* on their arrangement.[30] Thus our computed energy differences are correct only when we compare two structures with exactly the same composition and density. Realistically, for each structure considered, we ought to optimize the lattice constant to minimize the sum of $U_0$ and the structure energy, and then use the results to construct tie lines and determine the phase diagram. Fortunately, as just noted, we are mostly comparing structures of similar stoichiometry.

#### *3. Validity of pair form*

The calculation upon which our potentials were based went up to, but no further than, second order in perturbation theory. As a result, our cohesive energy includes only pair terms, which amounts to assuming that there is no directional bonding. There are at least two kinds of local atomic pattern for which this assumption is obviously questionable:

(a) Nearest-neighbor Mn contacts are taken into account only via an indirect hopping term mediated by the background electron sea.[31] Thus, our potentials are somewhat untrustworthy for Mn pairs and quite dubious for Mn triples. Fortunately, such clusters are rare in most of our structures, since the Mn atoms tend to be spread out uniformly in space; but for certain models with high $x_{\rm Mn}$, our structural energy may be far from the true one.

(b) Where a structure contains large perturbations such as vacancies, it is unreasonable to stop at second-order perturbation theory.[32] Indeed, one explanation for the stability of the ''Mackay icosahedron,''[33] and in particular for the vacant site at its center, uses a type of ''glue'' approximation, in which the structural energy has an additional term of the form

$$E_{\rm coh} = \sum_i F_i(\rho(\mathbf{x}_i)), \tag{6}$$

where $\rho(\mathbf{x}_i) = \Sigma_{j \neq i} \rho_j(R_{ij})$ represents the sum of the contributions of neighboring atoms to the electron density near atom $i$, and $F()$ is a *nonlinear* function.

### C. Relaxation procedures

For each model, we relaxed the initial configuration to a state of mechanical equilibrium with respect to the forces derived from the pair potentials. Models are ''topologically equivalent'' if they relax to exactly the same atomic structure. (It is assumed that the initial positions are close enough to the final ones that different relaxation algorithms give identical results.) We adopt the convention that superscript ''(0)'' refers to energies or positions before relaxation. Initial coordinates will be called ''ideal'' when they are linear combinations of the icosahedral basis vectors with integer or half-integer coefficients. Here we describe, not only our setup for relaxation computations, but also the use of calculated quantities relating to individual sites as criteria for the physical validity of the arrangements around those sites.

#### *1. Truncation of potentials*

To make the pair potentials more computationally tractable, we introduced a cutoff at a certain radius $r_{\rm cut}$. As in Ref. 9, each pair potential $V(r)$ was smoothed so that $V'(r)$ and $V''(r)$ were continuous everywhere and $V(r) = V'(r) = V''(r) = 0$ for $r \geq r_{\rm cut}$.

Models produced from 3/2 approximants and larger tilings (see Sec. IV B) are large enough that (using our truncations) no atom ever interacts with multiple images of another atom under the periodic boundary conditions; for smaller tilings, and for the real crystal structures of Sec. III, we form a sufficiently large supercell by joining copies of the unit cell.

Our preferred cutoff radius was $r_{\rm cut} = 11$ Å.[34] However, relaxations of large models (over $10^4$ atoms/unit cell) required excessive computer time with this cutoff; thus the majority of our relaxations were performed using $r_{\rm cut} = 6.2$ Å, which is chosen to just include the second-neighbor well, and (unless otherwise noted) the results in our tables and figures are from this truncation.

In many cases, we can partially relax a structure using $r_{\rm cut} = 6.2$ Å and then complete the relaxation using $r_{\rm cut} = 11$ Å, which results in very small readjustments. However, certain dense models which were (barely) stable with $r_{\rm cut} = 6.2$ Å, became unstable with $r_{\rm cut} = 11$ Å, and the energy differences between certain variants of the loose decorations (Sec. IV) changed sign. The small but significant differences between the results with 6.2 and 11 Å will be discussed in Sec. VII C.

#### *2. Relaxation algorithm*

Apart from a few molecular-dynamics runs (reported in Sec. VII A, below), all of our computations consisted of relaxations performed at zero temperature. Our relaxations were performed using a standard conjugate-gradient algorithm, except that the space group of the particular model was directly incorporated into the relaxation program, by constraining all symmetry-related atoms to relax together.[35] For a structure of high symmetry, the number of independent variables was thereby reduced by a factor of 10 or more.[36] A drawback of incorporating space-group symmetry into the relaxation is that spontaneous symmetry breaking cannot be detected.

The maximum time to relax one of our models was $\sim 4$ h CPU time on an IBM RISC-6000 workstation (for the $Pa\bar{3}$ ''8/5'' approximants). The criterion for convergence of the conjugate-gradient relaxation was that the energy change in one iteration be less than $\delta E = 10^{-8}$ eV per atom. The convergence rate can be a useful continuous diagnostic of stability, independent of the deviations from initial positions:

models which take exceptionally long to relax are often on the edge of instability.

#### *3. Stability criteria*

A common criterion for the stability of a model is that its structure does not amorphize upon relaxation, i.e., that the (angularly averaged) pair-distribution function retains sharp peaks out to arbitrarily large distances, indicating that long-range order is maintained. This criterion has been applied to assess the stability of 6D models.[9] The criterion that we adopt, however, is much stricter: we deem a model to be stable only if *every* atom stays within the sphere that is inscribed in its Voronoi polyhedron (each such sphere is thus in contact with its nearest neighbors). This criterion is motivated by our desire to obtain ''crystallographically correct'' decoration models (as discussed in Sec. II of paper I).

### D. Important motifs

A major objective of this paper is to understand the relationship between the form of the potentials and the atomic arrangements they favor. Some of these motifs are familiar in $\alpha$-AlMnSi and other crystalline Al-TM phases, such as regular Mn-Mn spacings of $\sim$4.6 Å, or $Al_{12}Mn$ icosahedra. These motifs, which influenced the proposed decorations, were reviewed in paper I and are rationalized below in Appendix A. After we present the relaxation results, we shall further discuss the relationship between the potentials and the patterns favored by them.

We next define our terms for three important structural features.

(i) The Mackay icosahedron (MI) consists of a $Al_{12}$ icosahedron around a central vacancy, with an outer shell composed of a large $Mn_{12}$ icosahedron and an icosidodecahedron of 30 Al atoms near the edges of that icosahedron.

(ii) All of our Al-Mn models include ''mini'' Bergman clusters, each of which consists of an $Al_{12}Mn$ icosahedron plus an outer shell of 20 Al/Mn atoms (each centered over an icosahedron face).

A ''pseudovacancy'' is a site with a negative vacancy formation energy: i.e., it is vacant in the ground state, but occupying it by an atom does not change the topology of the other bonds, does not make the model unstable, and does not force physically impossible bond lengths. (By contrast, a ''vacancy'' denotes a *defect* which costs energy relative to the ground state.) Pseudovacancies are frequent in known Al-Mn crystal structures;[37] a well-known example of a pseudovacancy is the MI center in $\alpha$-AlMnSi and $\alpha$-AlFeSi. They are the most important type of variation among closely related structure models, and are responsible for the lowered density in our loose family of models.

### E. Diagnostics: displacements and site energies

While revising our models to improve their energies (and eliminating those models which were unstable under relaxation, or too high in energy), we developed diagnostics to identify ''problem'' atoms and to compare alternate ways of resolving the uncertainties of extending the decoration. The displacement $D_i$ of atom $i$ from its initial position in the relaxation process serves as a diagnostic in practice: after all, if a certain atom displaces so far that the model must be deemed ''unstable,'' that atom (or one of its neighbors) is a prime candidate to be changed. However, $D_i$ should be interpreted with caution, since it depends on our (arbitrary) choice of ''ideal'' coordinates.

Another simple but useful diagnostic is the ''site energy''

$$E_i=\frac{1}{2}\sum_j V_{ij}(R_{ij}), \tag{7}$$

i.e., the part of the total pair energy (1) assigned to atom $i$.

Note that each site energy should be compared with the average for that chemical species; a site with $E_i$ far above this average is a prime candidate for a change in occupancy. To be precise, the site energy must be equal to or lower than the chemical potential for that species; otherwise the site would want to be empty. Consider the values

$$\Delta E_i(A)=E_i(A)-\mu_A, \tag{8}$$

where $E_i(A)$ means the site energy if species $A$ were placed on that site, with no additional relaxations. We can also consider $A=$ vacancy as another possible ''species,'' such that $\Delta E_i$ (vacancy)$\equiv 0$. Then the occupation adopted for site $i$ ought to be the choice $A_i^{\min}$ that gives the minimum of $\Delta E_i(A)$ over all $A$. Note that changing from some other option to $A_i^{\min}$ will certainly lower total energy, and this can only be lowered further when the system is re-relaxed to allow neighboring atoms to adjust to the change.

## III. SMALL CRYSTAL STRUCTURES

Before describing the main relaxations which were performed on CCT decoration models, we consider relaxations done using the same potentials and procedures (as explained in Sec. II), but applied to known crystal structures. In this section, we test the potentials on various crystal structures which are either Al-Mn alloys known from crystallographic refinements, or else structures arising in alloys of Al and other transition metals which have similar local order. Their unit cells are ''small'' only in comparison to the ''approximants'' which we treat in Sec. V; by any other crystallographic standard in condensed-matter physics, their unit cells would be considered rather large. Besides the $\alpha$-AlMnSi structure, which is the simplest approximant of our icosahedral Al-Mn decoration models, a number of these ''small'' crystalline structures are known to be decagonal quasicrystal approximants.

The purpose of the calculations on the Al-Mn phase diagram is to yield a level of confidence in the application of these potentials to structure determination in the quasicrystal problem. Explaining a phase diagram should mean not only accounting for the existence of the observed stable phases, but also for the nonexistence of the unobserved phases. Thus we included some real Al-Co and Al-Fe structures; since they have the same local motifs as Al-Mn structures, they are expected to have a better *a priori* chance of being low-energy than other unphysical structures we might devise (e.g., a solid solution).

TABLE I. Relaxation results for small crystal structures.

| Structure | Source | $x_{Mn}$ | $\rho_{at}$ (atoms/Å$^3$) | $E^0$ (eV/at) | $E_{rel}$ (eV/at) | $D_{max}$ (Å) |
|---|---|---|---|---|---|---|
| $Al_{12}Mn$ | Ref. 49 | 0.0769 | 0.06238 | 0.1993 | 0.1656 | 0.115 |
| $Al_6Mn$ | Ref. 48 | 0.1428 | 0.06427 | 0.0533 | 0.0418 | 0.100 |
| "$\alpha$-$Al_5Mn$"[a] | Ref. 46 | 0.1739 | 0.06801 | -0.0263 | -0.0730 | 0.251 |
| | DF1.1 | 0.1739 | 0.06801 | 0.1516 | -0.0733 | 0.303 |
| | DS3.1 | 0.1818 | 0.06505 | 0.0563 | -0.1228 | 0.314 |
| | DF1.3 | 0.2174 | 0.06801 | 0.0532 | -0.1937 | 0.381 |
| $Al_9Co_2$ | Ref. 41 | 0.1818 | 0.06699 | 0.5788 | [b] | |
| $\mu$-$Al_4Mn$ | Ref. 44 | 0.1957 | 0.06589 | -0.1731 | -0.1982 | 0.296 |
| $Al_3Mn$ | Ref. 39 | 0.2308 | 0.06765 | -0.2475 | -0.2817 | 0.396 |
| $Al_{10}Mn_3$ | Ref. 45 | 0.2308 | 0.06681 | -0.2822 | -0.2907 | 0.090 |
| $Al_{13}Co_4$ | Ref. 40 | 0.2353 | 0.07044 | -0.1906 | -0.2702 | 0.532 |
| $Al_3Co$ | Ref. 15 | 0.2553 | 0.06778 | -0.2712 | -0.2855 | 0.121 |
| $Al_{11}Mn_4$ | Ref. 43 | 0.2667 | 0.06919 | -0.3272 | -0.3437 | 0.271 |

[a]The "$\alpha$-AlMn" structure can be represented as a decoration of the pure "*A*" tiling (tiling $T1$), thus versions of it are associated with the corresponding decoration labels.
[b]Unstable.

### A. The structures

We test our pair potentials on realistic structures taken from both the AlMn and the AlCo systems, focusing on those that give rise to the low concentrations of Mn for which the pair potentials are applicable. Many of these phases are *not* stable in the Al-Mn system; however, they have local order similar to the Al-Mn phases, and differ only slightly in energy per atom from the real Al-Mn phases. Our aim is to determine whether the *signs* of these small differences agree with the real phase diagram, which was uncertain *a priori* in the light of some doubts about these potentials. This approach is similar to that taken by Ref. 14 in the Al-Co case.

The structures we chose[38] are listed in Table I, along with the Mn fraction $x_{Mn}$ and the atomic density $\rho_{at}$, from which the electron density may be computed via (2). For all structures except $Al_3Co$ we used the real reported lattice constant, since this gave an electron density $\rho_{el}$ close to the value $\rho_0$ for which our potentials are valid. In the case of $Al_3Co$, $\rho_{el}$ would be $\sim 7\%$ lower than $\rho_0$; thus in our results we chose a lattice constant so that $\rho_{el} \equiv \rho_0$.[39] Where the refinement indicated partial occupancy for an orbit, we tested only deterministic variants in which that orbit was either all filled or all vacant.

Several of these structures are approximants to decagonal phases. Hiraga's $Al_3Mn$ (Ref. 40) and the $Al_{13}Co_4$ phase[41] are good approximants — although the decagonal corresponding to $Al_{13}Co_4$ (Ref. 15) was discovered only recently. Also, $Al_9Co_2$,[42] $Al_{11}Mn_4$,[43,44] $\mu$(AlMn),[45] and the $Al_{10}Mn_3$ phase[46] may be viewed as imperfect approximants to decagonals.

The $\alpha$(AlMnSi) phase[47] is an approximant to an icosahedral quasicrystal, and as such it has been listed in later sections also as an approximant. The real $\alpha$-phase exists only with Si, but in our atomic model we replaced Si $\rightarrow$ Al. We did calculations for several variations of this structure, which were actually constructed by different decorations of tiling $T1$ (pure "*A*" cells). Finally, the $Al_6Mn$ (Refs. 48 and 49) and $Al_{12}Mn$ (Refs. 50 and 51) phases are not approximants in any meaningful way.

### B. Results of relaxations

Our potentials give a decent account of the Al-Mn phase diagram: they give a nearly correct picture of which phases are stable and which are not.

However, the version of $\alpha$ phase favored by our potentials is unphysical, in that it has Mn instead of a vacancy at the MI cluster center. Furthermore it has all of the $\delta$ sites vacant (implying bcc symmetry), whereas the real $\alpha$-AlMnSi structure has alternating occupancy (implying sc symmetry). We suspect that the first difference is an artifact of the deficiencies in our interatomic potentials (see Sec. II B); the second difference might be correct for a binary Al-Mn alloy — perhaps ternary or pseudobinary potentials adapted to Al-Mn-Si would have given a different answer.

For each structure, Table I gives the initial and final (relaxed) energy per atom and the maximum displacement $D_{max}$ of an atom from its initial position under relaxation. The majority of sites suffer only minor relaxations, but in some structures certain rogue atoms exhibit large displacements and/or changes in site energy; this indicates that the atomic arrangement in the vicinity is poorly matched with our potentials.

#### *1. Comparison with refinements*

There are three observations on the correlation between the behavior of structures under relaxation and the goodness of their refinements. First, the symmetry of a structure seems to be inversely correlated with the atomic displacements; e.g., they are small (about 0.1 Å) for $Al_{12}Mn$, $Al_6Mn$, and $Al_{10}Mn_3$, which are all highly symmetric structures with relatively few sites per unit cell. (This is not simply an artifact of our relaxation code, since we used supercells for all of our small structures.) Presumably the high symmetry has prevented atomic displacements in some directions.

Second, in the structures for which partial occupations were quoted, we observed that a change in the occupancy of just one site can produce drastic changes in the energy and stability of the model. The optimum deterministic choice for filling such sites relaxed almost as stably as did other struc-

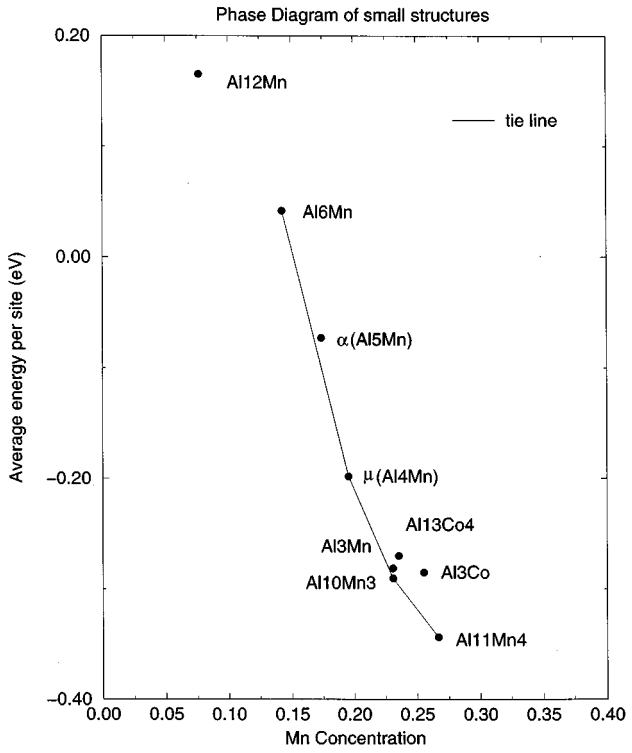


FIG. 2. Energy versus $x_{\mathrm{Mn}}$ for possible crystalline phases. Here "$\alpha$(A15Mn)" denotes $\alpha$(AlMnSi) with Si→Al. "$Al_3Co$" lattice parameters are rescaled to give the correct electron density $\rho_0$.

tures whose refinements quoted no partially occupied sites. For the cases in which the refinement showed several orbits with partial occupancies, we found that filling all of them gave an overpacked structure, yet zero occupancy was too loose. The best results were obtained when some but not all of the *orbits* were occupied. This suggests that our conclusions on the vacancy formation energies are roughly right on average for these alloys.[52]

Third, our calculations of relaxed positions could be considered as implementing the "synthetic" approach to structure determination suggested in paper I, in the sense that diffraction data and energy calculations are combined. In particular, in some cases we have taken a circa 1955 refinement (which is topologically correct as to the atom arrangement, but comparatively inaccurate in coordinates), and relaxed it to obtain a "synthesized" structure model. Indeed, our relaxed version was always closer to "reality" (as represented by a more modern refinement of the same structure) than the old structure was. This is a success for our potentials, but we do not know whether other potentials (e.g., the Morse potentials) might be equally successful (in correcting the cruder refinements).

#### *2. Phase diagram*

The resulting energies are plotted in Fig. 2. The solid line is the tie line between thermodynamically stable phases.

The $\alpha$-AlMn and $Al_{13}Co_4$ structures are predicted to be energetically unstable, while the $\mu$-$Al_4Mn$, $Al_3Mn$, and $Al_{10}Mn_3$ phases are predicted to be stable. All these predictions are correct except for the last: $Al_{10}Mn_3$ was wrongly computed to have a slightly lower relaxed energy than $Al_3Mn$. But since $Al_{10}Mn_3$ is the equilibrium phase at higher temperatures, the difference of the true cohesive energy between these phases must be small.

We have omitted drawing a tie line to the $Al_{12}Mn$ structure, which would have incorrectly implied $Al_6Mn$ was unstable; we suspect the $Al_{12}Mn$ energy is unphysically low, since this structure has the most extreme value of $x_{\mathrm{Mn}}$. We cannot just dismiss $Al_{12}Mn$, however, since it is within 1% of the target $\rho_{\mathrm{el}}$ and contains no dangerous Mn-Mn pairs. We would rather expect the potentials to be unrealistic at the Mn-rich end, the fact that our $Al_{11}Mn_4$ energy looks reasonable cannot be given much weight.

Figure 2 indicates the typical scale for energy differences between competing good structures. Stable phases lie below, and unstable phases lie above the tie line between competing phases, by 0.01–0.05 eV, exactly as in the Al-Co phase diagram.[14]

In conclusion, although the details in Fig. 2 are not perfect, the overall pattern of behavior suggests our potentials are realistic, and increases our confidence in their subsequent application (in Sec. V, below) to icosahedral structures in which we have no other way to discover the details.

## IV. DECORATION MODELS

We relaxed at least ten different variations for three families of MI-based decoration rule presented in paper I (loose SI, dense FCI, and dense SI). We attempted to systematically consider all possible decoration rules, within this narrow class. We did not test grossly different arrangements, e.g., placing Al and Mn atoms into a *i*-AlCuLi-type structure (which would almost surely be unstable).

Our variations all arise from the small set of "problem places" discussed in paper I. Most of the variations simply consisted of changing the occupancy or chemistry of a site (i.e., is it Al, Mn, or empty). Variations might also entail changing the structure topologically, by the alternation of one atom with a pair or triple of atoms; we found only one stable choice of this type (the $\gamma_{3Y}$ alternation in dense models).

In the course of testing our models, we tried many other variants involving either other chemistry/occupancy combinations in the variable places mentioned here, or variations in places other than mentioned here. [An example of the latter would be replacing Al($\gamma_{3D}$) by 3 Al($\gamma$) atoms.] However, most of these adjustments were discarded on the grounds that they were unstable, or led to unacceptably high site energies.

### A. Definitions

By "model" we mean a combination of a particular tiling and a particular decoration. (For six-dimensional models, it means a particular cut through a particular 6D hypercrystal.)

In this paper, we focus on decoration models: in a "decoration," atoms are placed on tiling objects such that both

(i) every object of a given type is decorated in the same way (just like a unit cell in ordinary crystallography), and

(ii) the point-group symmetry of a decorated tiling object is the same as that of the "bare" tiling object before decoration.

TABLE II. Approximant tilings used for decoration.

| Code | Tiling | Space group | $N_{\text{node}}$ | $N_A$ | $N_B$[a] | $N_D$ | $N_E$[a] |
|---|---|---|---|---|---|---|---|
| $T1$ | Pure $A$ | $Im\bar{3}$ | 2 | 12 | 0 | 0 | 0 |
| $T2$ | Pure $EC$ | $R\bar{3}m$ | 1 | 0 | 0 | 0 | 1 |
| $T3$ | Pure $D$ | $P\bar{3}m1$ | 1 | 0 | 0 | 2 | 0 |
| $T4$ | "$\tau^3$ OR"[b] | $R3m$ | 3 | 6 | 3 | 1 | 0 |
| $T5$ | Cubic 2/1 | $Pa3$ | 8 | 24 | 0 | 0 | 4 |
| $T6$ | Cubic 3/2 | $Pa3$ | 32 | 72 | 24 | 8 | 4 |
| $T7$ | Cubic 5/3 | $P2_12_12_1$ | 136 | 312 | 88 | 32 | 24 |
| $T8$ | Cubic 5/3 | $P2_13$ | 136 | 312 | 48 | 32 | 44 |
| $T9$ | Cubic 5/3 | $R\bar{3}$ | 138 | 348 | 60 | 24 | 38 |
| $T10$ | Cubic 8/5 | $Pa3$ | 576 | 1320 | 312 | 136 | 132 |
| $T11$ | Cubic 8/5 | $Pa3$ | 592 | 1608 | 216 | 72 | 180 |

[a] $N_C = N_B + 2N_E$.
[b] Name used in Ref. 8.

An "atomic site" is a position in space to which a "chemistry" is associated. (See Sec. II A of paper I.) Atomic sites that decorate a given tiling object are said to be "bound" to that tiling object. Condition (ii) above forces atomic sites to lie in discrete orbits, generated by the point-group symmetry of the objects to which they are bound. The association of these orbits to tiling objects is called a "binding." The specific coordinates of atoms, generated in this fashion, will be called the "canonical positions" for that model and binding.

Our decoration models are based on the "canonical-cell tiling" (CCT).[8] This is built out of four kinds of cells, denoted "$A$, $B$, $C$, $D$," such that their vertices ("nodes") are joined by a network of "linkages" in both twofold and threefold directions. The former linkages are called $b$ linkages, the latter are called $c$ linkages. The three different sorts of faces are labeled by the letters $X$, $Y$, and $Z$. In this work, we treat the threefold symmetric pair of $B$ cells as an additional cell "$E$." Together, these comprise a set of "tile objects" for the CCT. (The objects are seen in Fig. 1 of paper I.)

### B. CCT approximants

As periodic boundary conditions are preferable for doing simulations/relaxations (due to the absence of surface effects) we use large periodic packings of canonical cells called "approximants." These approximate the corresponding extended, icosahedrally symmetric quasicrystal.[53] The small approximants are very imbalanced with regard to tile content; and even the larger approximants, owing to their high symmetry, under-represent some of the ways two tiles can adjoin. Since a given trial decoration might be good for some of these ways and bad for others, we therefore need to test out our decoration models on a broad selection of canonical-cell approximants.

We selected the 11 reference canonical-cell tilings of canonical cells listed in Table II. The labeling "$p/q$" means that the unit cell is the same size as a "true" $p/q$ approximant of the (as yet hypothetical) icosahedral canonical-cell tiling.[7] The first (and smallest) six approximants appear in Ref. 8, Table VII. The 5/3 tilings are taken from the known exhaustive list of all 30 inequivalent 5/3 approximants, discovered through exact enumeration, reported in Ref. 54. Lastly, the 8/5 tilings are from Ref. 55; these were discovered as the final states of Monte Carlo annealing simulations, that attempted to maximize the packing fraction. When decorated with atoms, the largest models (decorations of the "8/5" tilings) contain $\sim$43 000 atoms each.

Our large "5/3" and "8/5 "tilings were judiciously chosen to have high symmetry (as demanded by the relaxation procedures[56]) and to vary the following degrees of freedom:

(i) The variance of the perp-space[57] coordinate of the tiling nodes. This should be smallest in a true approximant of the (as yet unknown) ideal quasiperiodic CCT. The perp-variance is low for tilings $T7$, $T9$, and $T10$, and is high for tilings $T8$ and $T11$.

(ii) The relative fraction of space occupied by $D$ cells (at the expense of $A$ cells).[58] The number density of nodes (and hence of MI's) increases with the density of $A$ cells; if the nodes were decorated by identical spheres, their packing fraction would range from 0.600 to 0.625 (for icosahedral symmetric structures).[54,55] Tilings $T9$ and $T11$ were chosen to have high density.

### C. Families of decoration rules

In paper I, we presented four basic families of sensible CCT decoration rules. In resolving the most problematic sites, we identified several possible resolutions, thus creating a number of variants within each family. The results of the present paper derive from relaxing and comparing these variants.

We have labeled the different decoration rules as e.g., "DF$n.x$;" here the first letter is "D" or "L" for "dense" or "loose" family of decorations, the second letter is "F" or "S" for "FCI" or "SI" symmetry decorations. Within each of these four families, we have independent ways of varying the density and the chemistry of atomic orbits. The number $n$ labels variants with different total number density and the number "$x$" labels variants of different $x_{\text{Mn}}$.

#### *1. Loose model variants*

Based on the problem sites identified in paper I, Sec. IV, we adopted variants of loose SI models as listed in Table III.

TABLE III. Variant decorations.

| Decoration | $\delta_Y$ | Al($\gamma_Z$)[a] | $\gamma_{3D}$ |
|---|---|---|---|
| LS1.1 | Al | 6/6 | Mn |
| LS1.2 | Mn | 6/6 | Mn |
| LS2.1 | Al | 4/6 | Mn |
| LS2.2 | Mn | 4/6 | Mn |
| LS2.3 | Al | 4/6 | Al |
| LS2.4 | Mn | 4/6 | Al |
| LS3.1 | | 4/6 | Mn |
| LS3.2 | | 4/6 | Al |

[a]Site $\gamma_Z$ is always Al.

The ''problem sites,'' which we recall are candidates for modifications, occur in three orbits:

(i) one ''$\gamma_{3D}$'' near the center of each $D$ cell;

(ii) one ''$\delta_Y$'' near the center of each $Y$ face;

(iii) six ''$\gamma_Z$'' sites form a ring around the center of each $Z$ face, (which straddles the $Z$ face).

The $\gamma_{3D}$ and $\gamma_Z$ ''problem'' sites are in fact the Al sites with highest site energies, *excluding* the MI sites (we have not allowed variations within the MI). Thus they are promising places to try some other occupation. Indeed, Mn($\gamma_{3D}$) has site energy similar to Mn($\nu$), which we have assumed is always Mn.[59,60]

The six ''Al($\gamma_Z$)'' sites decorate not only the $Z$ faces on $D$ cells, but also are found around the center of each $E$ cell (which can be considered as having an internal $Z$ face). When all six Al atoms are present, they have the highest Al site energies (outside of the MI). We concluded that this configuration was slightly overpacked, so we tried variants in which some of those sites were vacant, labeled ''6/6,'' ''5/6,'' and ''4/6'' by how many sites are occupied. Trials with small models indicated that the ''4/6'' arrangement was considerably better than the ''6/6'' variant, and this was later confirmed in our systematic comparisons.[61–63]

The ''$\delta_Y$'' site was sensitive to the truncation of the potential — the Mn($\delta$) site energy is *lower* than that of Mn($\nu$), but with the shortened cutoff $r_{\rm cut}=6.2$ Å, Mn($\delta$) came out *higher*. (The results and explanation are discussed in Sec. V A 2 and Sec. VII C; example site-energy results are in Table V.)

#### 2. Dense FCI variants

In dense models the density variation is associated purely with the $\gamma_{3Y}\leftrightarrow 3\,\gamma$ alternation, as noted in paper I. These are $\gamma_{3Y}$ sites associated with the *odd Y* faces; they can occur in odd $B$, even $D$, or $E$ cells. (In all our models, there was no such freedom for the $\gamma_{3D}$ sites.) We decided on *three* density variations that independently treat these locations:

$n=1$ is the loosest, assigning a single Al($\gamma_{3Y}$) atom in every case.

$n=2$ is the densest, with three Al($\gamma$) atoms replacing the $\gamma_{3Y}$ sites in every case.

$n=3$ tries to account for the local atomic density, assigning a single Al($\gamma_{3Y}$) when the site falls in an even $D$ cell, but replacing the site by 3 Al($\gamma$) when it is in an odd $B$ or an $E$ cell.

The chemical variations were performed on a certain subset of $\delta$ sites which reasonably allows either Al or Mn. These were the $\delta_b$ sites on odd $b$ linkages that fell within $B$ and $D$ cells [to be called $\delta_b(B)$ and $\delta_b(D)$], as well as the $\delta_D$ sites in the $D$ cell. The two chemical variants are then $x=1$ and $x=2$, which, respectively, assign the above-mentioned $\delta$ sites to be either all Al or all Mn.

A ''modified'' DF2.1 rule differs from the case $n=2$ above in setting all $\delta_b(D)$ sites vacant. (This was found necessary to stabilize the pure $D$ tiling under Morse potential relaxations.)

#### 3. Dense SI variants

All density and chemical variations were on the $\delta$ sites. $\delta$ sites may occur in $b$ linkage, $Y$ face, and $D$ cell. In dense SI models, as outlined in paper I, we are forced to differentiate three kinds of $b$ linkage, namely $b(A_4)$, $b(A_2)$, and $b(A_{CC})$.

Our density variations involve the occupancy of the $\delta_b(A)$ and $\delta_Y$ type sites, but never the occupied $\delta_D$ sites:

$n=1$ sets all $\delta_b(A)$ occupied and all $\delta_Y$ vacant.

$n=2$ is the densest, with all $\delta_Y$ and most $\delta_b(A)$ being occupied, and only the $\delta_b(A_{CC})$ being left vacant.

$n=3$ is the loosest, occupying only $\delta_b(A_2)$ and $\delta_b(A_{CC})$. This differs from the $n=1$ option only through making the $\delta_b(A_4)$ site vacant.

Chemical variations are implemented only on the $\delta$ sites:

$x=1$ sets all $\delta$ sites to Al;

$x=2$ sets only the $\delta_b(A_2)$ sites to Al, and the rest of the occupied $\delta$ sites to Mn.

#### 4. Loose FCI models

It is possible (paper I) to generate loose CCT models with FCI order, which would be analogs of the quasiperiodic modified-Katz-Gratias (KGme) model studied in Ref. 64. (Such models may be a good starting point for CCT models of alloys with FCI order such as $i$-AlPdMn.)

We did not include any FCI loose models in our systematic study. A few examples were checked in passing (subsets of even $\delta$ sites were occupied). From these we confirmed that the results of FCI and SI loose models differ in just the same way that those of their 6D analogs [FCI KGme model and SI Duneau-Oguey (DO) model] did; in particular, the SI models had lower energy.

### D. Procedures and diagnostics for variants

Each of the model variants was systematically applied to each of the 11 CCT ''approximant'' tilings to generate a model. Average behavior across the 11 tilings suggest properties intrinsic to the variant decoration. Since we focus on atomic orbits rather than individual atoms, we elaborate on our methods for evaluation of orbits and consequently decorations.

*RMS deviations.* After each relaxation of a decoration model, we computed the ''canonical positions'' (see definitions in paper I, Sec. II) from the relaxed coordinates for each orbit of atoms. This means that, for each site of an orbit bound to tiling objects of type $O$, we apply the inverse space operation which maps its object back onto the reference tile

of type $O$; then the canonical position is the mean of the cloud of these points, and the canonical rms is their standard deviation.[13]

Note that this rms is invariant if the initial structure is changed, as long as it is topologically equivalent; in particular, it has nothing to do with our choice of ''ideal coordinates.'' On the other hand, the rms is specific to a particular ''binding'' of the sites; making the ''binding'' more elaborate (thus increasing the number of fitting parameters) *decreases* the rms, even when the actual relaxed structure is unchanged. It should be noted that the distortions of the tiles themselves (equivalently, displacements of the centroids of clusters decorating the tile nodes) contribute an additional term to the canonical rms value of every orbit.

In contrast to stability under relaxation (Sec. II C) or the single-site energy (Sec. II E), the rms is not a physical criterion for how well the orbit in question reduces the total structural energy. Rather, it is a criterion for the usefulness of the binding chosen for that orbit; the overall mean rms estimates the validity of a decoration picture at all, measuring the components of the (relaxed) atom positions which *cannot* be accounted for in the decoration model. A small value for the rms (for a simple enough binding) means that the atom positions can be adequately represented without much ''context dependence,'' i.e., they are not strongly dependent on the surrounding tile configurations.

There is one way in which the rms can indirectly guide us to a reduction of energy. If the rms is large, it suggests there are qualitatively different kinds of sites in the orbit. Then it may be advantageous to ''rebind'' (see paper I) the orbit, i.e., to differentiate it into two or more distinct new orbits. Then it is possible for the new orbits to have different occupations, which may improve the energy.

## V. RESULTS

This section gives the core results of our relaxations. For each group of models reported on, we will first discuss the stability (or lack thereof) of the atomic positions under the relaxation. Then we turn to the main issue, the energies, our main concern being which variant model is optimal, i.e., which one lies closest to the convex tie line in a plot of $x_{\mathrm{Mn}}$ versus energy. We correlate these energies with the many directions in our parameter space: some of these concern the decoration rule — either the overall family (dense/loose, FCI/SI), or the variations on specific sites (affecting $n_{\mathrm{at}}$ and $x_{\mathrm{Mn}}$); other directions concern the potentials in use — in this section, this means changing the truncation radius $r_{\mathrm{cut}}$. As noted in Sec. II, it is more correct to use $r_{\mathrm{cut}}=11$ Å, but most of our systematic comparisons use $r_{\mathrm{cut}}=6.2$ Å since it is too costly to relax all the models with the longer cutoff.

Left to later sections (VI and VII) are yet other directions in the parameter space, which have been explored less thoroughly. We have also left most of the discussion of these results to later sections, in particular Sec. VIII. Our main finding is that loose models are good, in having energies offset by a small constant above the equilibrium tie line, comparable to the energy difference among crystalline structures seen in Sec. III, and that different loose variants have rather similar behavior. We also have found that a decoration approach accounts rather well for the relaxed positions (Sec. V B). On the other hand, in the case of the dense models, none of the just-mentioned findings is valid (Sec. V C).

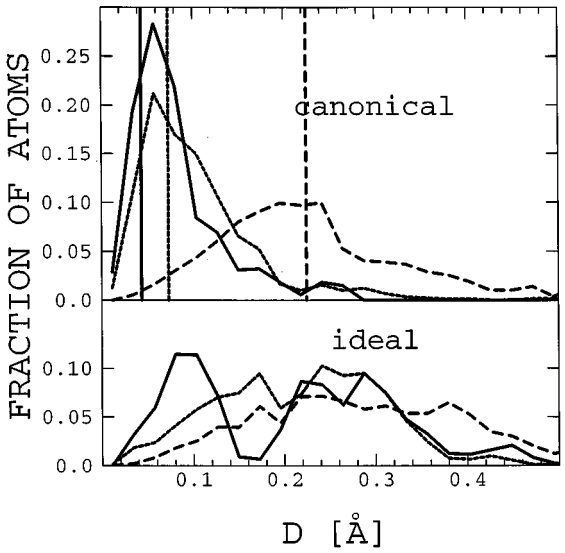


FIG. 3. Distribution of atomic displacements $D$ from ideal to relaxed (bottom) and from ''canonical'' to relaxed (top) atomic positions. Solid line: Loose model LS1.2 under 11 Å cutoff. Dotted line: Dense model DF2.1 under 6.2 Å cutoff. Dashed line: Dense model DF2.1 under 11 Å cutoff. The histogram includes Al and Mn atoms together. The bin resolution on the $x$ axis is $0.005a_q$. Vertical bars mark the rms displacements of the MI centers (CCT nodes), which limits the crystallographic accuracy of the CCT model.

### A. Results of loose models

Using the long-range potentials with $r_{\mathrm{cut}}=11$ Å, all decoration rules (and variants) were relaxed for tilings $T1-T6$, and furthermore rules LS1.2 and LS2.4 (which seem to be optimal) were relaxed with the 5/3 approximants (tilings $T7-T9$). However, since our relaxations with the shorter cutoff $r_{\mathrm{cut}}=6.2$ Å were more systematic and complete, most of the data presented here are taken with that cutoff.

#### *1. Stability*

Our results demonstrate clearly the plausibility of MI-based models under realistic pair potentials. To our surprise, every model in the loose family was found to be remarkably stable, as seen in Fig. 3. Indeed, the peaks in the pair-distribution function (PDF) at large $r_{ij}$ are just as sharp in large tilings as in small ones. The Mn-Mn correlations (see Fig. 4) are especially striking.[66]

Furthermore, the typical rms displacement of the relaxed positions from the ''canonical'' positions for each orbit was only 0.08–0.09 Å for the largest tilings studied; a sample histogram is included in Fig. 3. Table IV compares the configurations before and after relaxation, for the atom types in the two-shell Mackay icosahedron. The displacements for Mn(0) (which is occupied in all these models) and the inner Al($\alpha$) shell are presumably following rigid motions of the entire cluster (responding to phonon-phason coupling — see Sec. VII B). Since our sort of decoration model has no way to describe a net displacement of an entire MI, we must hope

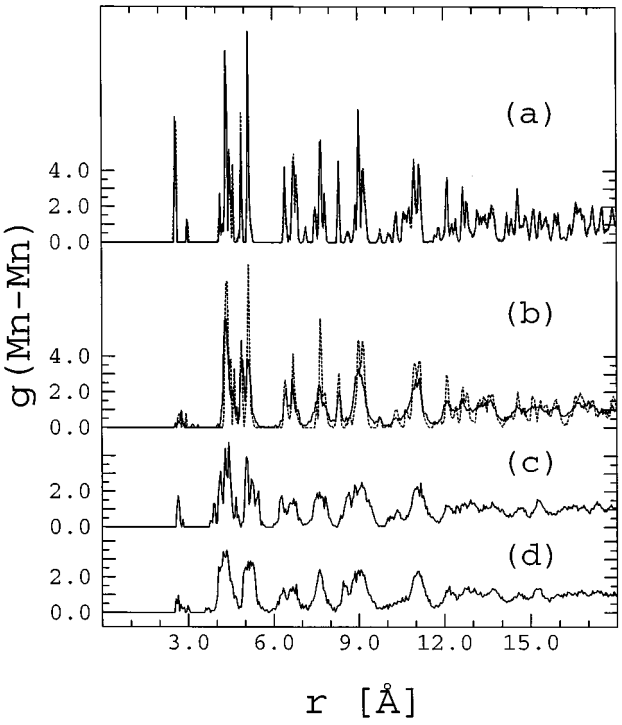


FIG. 4. The Mn-Mn pair distribution function for various CCT decoration models. (a) Loose 5/3 T4 LS1.2 (solid line 11 Å cutoff, dashed 6.2 Å); (b) Dense 5/3 *T*4 DF2.1 (solid line 11 Å cutoff, dashed 6.2 Å); (c) the same as (a), but under Morse potentials; (d) the same as (b), under Morse potentials.

that these are small and indeed the table shows $\sigma_i \sim 0.03$ Å.

The expansion/contraction of the MI, relative to ''ideal'' positions, is similar to the experimental finding for *i*-AlMnSi.[67] The inner Al($\alpha$) and outer Mn($\mu$) icosahedra expand, while the icosidodecahedron formed by Al($\beta$) contracts relative to the ideal positions.

### *2. Energies*

The site energies for the different orbits, are shown in Table V. It may be seen that the Mn site energies *increase* from the MI center towards the third shell and the tile interior regions, [along the sequence Mn(0), Mn($\mu$), Mn($\nu$), Mn($\delta$)]. On the other hand, the Al site energies typically *decrease* along the sequence Al($\alpha$), Al($\beta$), Al($\gamma$), i.e., inside to outside. [In the MI, as Table IV shows, the site energy variance follows the trend of the canonical rms: it is largest for the outermost and most distorted Al($\beta$) shell.]

TABLE IV. Relaxation of MI cluster: distortions and site energies.

| | $R_i$(Å) | | | | |
|---|---|---|---|---|---|
| Shell[a] | (expt.)[b] | (calc.) | $\phi_i$ (Å) | $E_i^{(0)}$ (eV) | $E_i$ (eV) |
| Mn(0) | (0) | 0 | 0.038 | -2.029 | -2.020 |
| Al($\alpha$) | 2.45 | 2.525 | 0.039 | 0.241 | 0.244 |
| Mn($\mu$) | 4.90 | 4.896 | 0.034 | -1.437 | -1.450 |
| Al($\beta$) | 4.60 | 4.769 | 0.104 | 0.133 | 0.120 |

[a]Decoration LS1.1 on tiling *T*6. $r_{\rm cut}=6.2$ Å.
[b]Reference 65.

TABLE V. Site frequencies and site energies.

| | | $E_i$ (eV) | |
|---|---|---|---|
| Site[a] | Percentage | ($r_{\rm cut}=6.2$ Å) | ($r_{\rm cut}=11.0$ Å) |
| Mn(0) | 1.31 | -2.0155 | -1.7975 |
| Mn($\mu$) | 15.74 | -1.4390 | -1.6643 |
| Mn($\nu_Y$) | 1.62 | -1.3307 | -1.4190 |
| Mn($\nu_D+\gamma_{3D}$) | 1.23 | -1.4000 | -1.5873 |
| Mn($\delta$) | 1.62 | -1.1001 | -1.5546 |
| Al($\alpha$) | 15.74 | 0.2463 | 0.1994 |
| Al($\beta$) | 39.35 | 0.1019 | 0.0899 |
| Al($\gamma_Z$) | 6.71 | 0.1001 | 0.0681 |
| Al($\gamma_b$) | 15.74 | -0.0289 | -0.0499 |
| Al($\gamma_D$) | 0.93 | -0.2188 | -0.2535 |
| Al($\delta_Y$)[b] | 1.62 | 0.1395 | |
| All Mn (combined) | 21.53 | -1.4382 | -1.6413 |
| All Al (combined) | 78.47 | 0.1007 | 0.0779 |

[a]Decoration LS1.2 on tiling *T*8.
[b]This site energy is from decoration LS1.1, since model LS1.2 has no $\delta$(Al) sites. (The other site energies in LS1.1 are similar to those shown above, the largest differences being at the immediate neighbors of the $\delta_Y$ site.)

Figure 5 plots the (relaxed) energy/atom against $x_{\rm Mn}$, for the different models. The overall slope in such a plot just shows the difference between the Al and Mn chemical potentials. To help compare models with differing $x_{\rm Mn}$ content, we have drawn the (solid) tie line (same as in Fig. 2) and a (dashed) reference line.

The equation of the reference line is

$$E=\mu_{\rm Al}^{\rm ref}(1-x_{\rm Mn})+\mu_{\rm Mn}^{\rm ref}x_{\rm Mn}. \tag{9}$$

Here we take this to be the best linear fit of the 11 models produced by decoration rule LS2.4. We obtain

$$\mu_{\rm Al}^{\rm ref}=0.3186, \quad \mu_{\rm Mn}^{\rm ref}=-2.2392 \tag{10}$$

for $r_{\rm cut}=6.2$ Å.

It is necessary to compute a separate line (also using LS2.4) for the $r_{\rm cut}=11$ Å case, since the slope is different:

$$\mu_{\rm Al}^{\rm ref}=0.3793, \quad \mu_{\rm Mn}^{\rm ref}=-2.7437 \tag{11}$$

for $r_{\rm cut}=11$ Å.

As can be seen from Fig. 5, the best decoration rules for $r_{\rm cut}=6.2$ Å are ''LS3.1'' and ''LS3.2'' (which have very similar energies) All tilings from these two rules lie almost exactly on a straight line parallel to the reference line (10). At $r_{\rm cut}=11$ Å, the plot would look quite similar, with a different reference line, but the best models are now LS1.2 and LS2.4 (the reason for this difference is discussed in Sec. VII C).

Table VI summarizes all our results for $r_{\rm cut}=6.2$ Å, using tiling *T*7 as a representative example. [Although it is an important parameter, the conduction-electron density $\rho_{\rm el}$ is not displayed since it may be found from the Table VI entries using Eq. (2).]

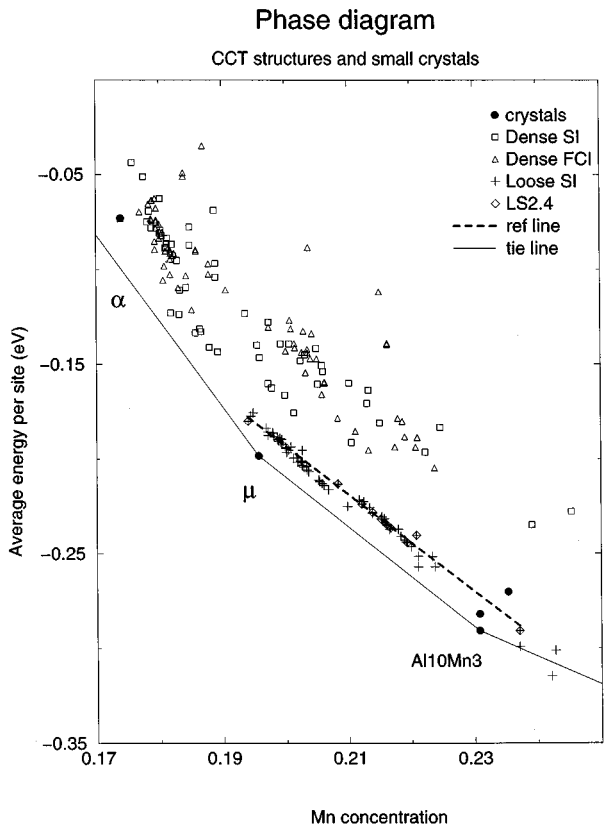


FIG. 5. Energies versus $x_{\mathrm{Mn}}$ for various CCT decoration rules. The small crystal structures from Fig. 2 are repeated here as heavy dots, as is the tie line. The dashed line is the reference line Eq. (10) for quasicrystal decorations, and effectively connects models LS2.4-*T*1 and LS2.4-*T*3. Points from LS2.4 (all 11 tilings) are shown as diamonds, to illustrate how the energies from a single loose decoration fall nearly on a straight line.

There is no unique way to decide whether one decoration rule is ''better'' than another, especially since a rule may be good on some tilings and poor on others. One good way would be to fit a line for each decoration rule through the points in Fig. 5 representing the models made using tilings $T1-T11$, and to see which fit lines are lowest in the interesting range of $x_{\mathrm{Mn}}$. For a simpler, but somewhat more arbitrary way, one first adopts a particular representative tiling and represents each rule by its energy for that tiling; then one adopts a single reference line on the plot in Fig. 5, characterizing each rule by its difference from that line (e.g., the entries in Table VII). The conclusions of the simpler way are well-defined to the extent that the different fit lines have the same slope (which is an good approximation for the loose models.)

TABLE VI. Comparison of decoration model results.

| Model[a] | $\rho_{\mathrm{at}}$ (Å$^{-3}$) | $x_{\mathrm{Mn}}$ (Å$^{-3}$) | $\bar{\sigma}$ (Å$^{-3}$) | $E_{\mathrm{rel}}$ (eV/at) |
|---|---|---|---|---|
| LS1.1 | 0.06718 | 0.1991 | 0.080 | -0.1891 |
| LS1.2 | | 0.2153 | 0.089 | -0.2306 |
| LS2.1 | 0.06599 | 0.2027 | 0.087 | -0.2018 |
| LS2.2 | | 0.2192 | 0.097 | -0.2438 |
| LS2.3 | | 0.1995 | 0.086 | -0.1924 |
| LS2.4 | | 0.2160 | 0.095 | -0.2346 |
| LS3.1 | 0.06490 | 0.2061 | 0.086 | -0.2139 |
| LS3.2 | | 0.2029 | 0.084 | -0.2043 |

[a]Using tiling *T*7, $r_{\mathrm{cut}}=6.2$ Å.

TABLE VII. Effects of potential truncation.

| Model[a] | $\Delta E$ (meV/atom)[b] ($r_{\mathrm{cut}}=6.2$ Å) | ($r_{\mathrm{cut}}=11.0$ Å) |
|---|---|---|
| LS1.1 | 4.7 | 5.5 |
| LS1.2 | 8.9 | -0.1 |
| LS2.1 | 1.8 | 4.1 |
| LS2.2 | 6.5 | -1.2 |
| LS2.3 | 2.4 | 4.4 |
| LS2.4 | 6.8 | -0.9 |
| LS3.1 | -0.7 | 2.6 |
| LS3.2 | -0.1 | 2.8 |

[a]Using tiling *T*6 for all models.
[b]Energy relative to reference lines (10) and (11).

To make generalizations as to which option is optimal at each variable site, we can then correlate the differences in the resulting energies with the options shown in Table III. Indeed, it appears that the cost of different options is simply additive, so that we can assign an independent energy cost for each ''problem'' place. By this analysis, Table VII suggests that ''LS2.2'' and ''LS2.4'' are the overall best models (with $r_{\mathrm{cut}}=11$ Å); however, under the shortened cutoff (6.2 Å), the best ones are LS3.*x*.

Separated by the three variable types of site, the conclusions are

(i) In $\delta_Y$ sites, the competition between the options Al/Mn/vacancy ''loose'' models is ''delicate,'' in that the energy differences are small and so the optimal choice can depend on other minor features, e.g., the long-distance tails of the potentials. The energy differences are read off from the entries LS.2.1, LS.2.2, and LS.3.1 in Table VII, since these rules differ exclusively in their $\delta_Y$ occupation. For $r_{\mathrm{cut}}=11$ Å, the best option is Mn (as in LS2.2); the excitation cost (per $\delta_Y$ site, with the aid of Table VIII) is 0.32 eV for Al and 0.23 eV for vacancy. On the other hand, under the shortened 6.2 Å cutoff, this order is reversed: the best option is vacancy (as in LS3.1). Under $r_{\mathrm{cut}}=6.2$ Å, the excitation cost is $\sim$0.15 eV for Al and $\sim$0.43 eV for Mn.

TABLE VIII. Models used for molecular dynamics.

| Decoration[a] | $N_{\mathrm{atoms}}$ | $x_{\mathrm{Mn}}$ |
|---|---|---|
| DS2.1 | 2488 | 0.1801 |
| DS2.2 | 2488 | 0.2058 |
| LS1.1 | 2448 | 0.1993 |
| LS1.2 | 2448 | 0.2157 |
| LS2.1 | 2400 | 0.2033 |
| LS2.2 | 2400 | 0.2200 |
| LS3.2 | 2360 | 0.2034 |

[a]All of these with tiling *T*6. Atom density is $\rho_{\mathrm{at}}\equiv N_{\mathrm{at}}/V_{\mathrm{cell}}$, with cell volume $V_{\mathrm{cell}}=(\tau^2 b)^3=374.3a_q^3=3.643\times10^4$ Å$^3$.

(ii) The $Z$ face ($\gamma_Z$) sites are better in the ''4/6'' decoration than in the ''6/6'' decoration. (The two vacant sites are on the $Z$ face, along its twofold symmetry axis.) By comparing the relaxed energies of LS1.1/LS1.2 and of LS2.1/LS2.2, we can estimate the excitation energy of filling each *pair* of $\gamma_Z$ vacancies to be 0.13 eV for $r_{\rm cut}=11$ Å (or 0.28 eV for $r_{\rm cut}=6.2$ Å).

(iii) The $\gamma_{3D}$ site is better with Mn under our potentials (which are, however, least reliable for that site[59]), but the excitation cost of Al is small. Using Table VII, it is found to be 0.09 eV per $\gamma_{3D}$ site (or 0.17 eV, for $r_{\rm cut}=6.2$ Å).

### B. Tests of averaged positions

For each decoration rule, the ''canonical'' positions for each orbit were computed as a sort of symmetrization or average of the relaxed positions. The rms deviations from the average position (see Table IV) were an obvious measure of the goodness of the decoration description, in particular for diffraction which is sensitive to the displacements.

As can be seen in Table VI, the loose models have rms deviations of $\bar{\sigma}\sim 0.1$ Å or less. [Typically, the Al($\beta$) orbit has rms$=0.11$ Å and all other orbits have much less.] It indicates that the simplest (''minimal'') binding of the CCT decoration can already capture the relaxation displacements rather well.

The Al($\beta$), the MI second-shell atoms, have a rms much larger than any other orbit, presumably because these atoms are exposed to a greater variety of environments. A site ''bound'' to a cell, if it is near the cell's face, can ''see'' only two or so possible neighboring cells. On the other hand, the outer MI atoms may fall into any of the nine different kinds of corner of a canonical cell.[68]

This confirms that a decoration model (the one with ''canonical'' averaged positions) may give a good approximation of the true minimal energy positions. This observation might justify a shortcut to computing the ''tile Hamiltonian'' (energy of one tiling as opposed to another), by evaluating the total interatomic pair energy directly from the unrelaxed ''canonical'' positions (rather than from tile-tile terms fitted to the relaxed energies of representative tilings, the approach sketched in Sec. IX).

For every quantity computed from positions, we can construct an analogous one from the site energies. For example, in analogy to the canonical positions, we earlier defined canonical energies by averaging $E_i$ over each orbit. So also for each orbit there is a corresponding variance $\sigma_E^2$, which serves to quantify how similar are the local environments of different sites in that orbit, as reflected in the site energies. We let $\bar{\sigma}_E^2$ be the mean of $\sigma_E^2$ over all orbits (weighting each atom in the orbit equally). These quantities are shown in Table IX for a typical loose decoration applied to two selected tilings.

Yet another way of testing the canonical positions is to see whether computing the energy commutes with the canonical averaging over an orbit. In Table IX, we compare the average energy per atom for *unrelaxed* model using the ''canonical'' positions, $E_0^{\rm can}$, with the canonical average of the *relaxed* energy $E_{\rm rel}$. It can be seen from Table IX that

TABLE IX. Energies from unrelaxed canonical positions.

| Tiling[a] | $x_{\rm Mn}$ | $E_0^{\rm can}$ (eV/atom) | $E_{\rm rel}$ (eV/atom) | $\bar{\sigma}_E$ (eV/atom) |
|---|---|---|---|---|
| $T6$ | 0.2000 | -0.17840 | -0.19381 | 0.03115 |
| $T8$ | 0.1987 | -0.17731 | -0.18976 | 0.03049 |

[a]Rule LS2.3 for each tiling.

$\Delta E\equiv E_0^{\rm can}-E_{\rm rel}$ is $\sim 0.015$ eV. This is reasonably small [the typical energy scale of differences among different tilings is $\sim 0.01$ eV/atom).

### C. Results of dense models

The dense SI and FCI families of decoration rules were applied to tilings $T1$–$T9$.[69] These models are worse than loose models in all aspects of their behavior: some of them have less stability, all of them have higher energies, and the tile Hamiltonian concept would not work. Some other trends will be explained by microscopic details of the ''problem sites.''

#### *1. Stability*

Most of DS and DF structures are structurally stable for small tilings, but not in the case of larger (size 5/3) approximant tilings. Only a third of decoration rules lead to stable structures (see Fig. 3); even in these rather stable dense models, the rms is strikingly larger than it is in loose models. Another third have a few orbits of runaway atoms, so that the canonical rms for those orbits can be larger than 0.2 Å. The remaining third of the rules produce so many runaway orbits that the relaxation program cannot find even a local minimum of the energy.

#### *2. Energies*

The dense models do not cluster neatly along straight tie lines as the loose ones do, as can be seen in Fig. 5. Thus one can distinguish certain models with the lowest energy (compared to the crystalline phase tie line); these occur around $x_{\rm Mn}=0.20$ (which happens to be the physically correct concentration for $i$-AlMn).

A least-squares fit line through all of the dense models gives nearly the same slope as for the loose models. This justifies defining ''net'' energies for comparison purposes (as in Table VII) by subtracting off the same reference line (10) (for data at $r_{\rm cut}=6.2$ Å). Then the best dense (FCI) rules DF1.1 and DF1.2, applied to the tiling $T7$, give energies 0.042 and 0.035 eV, respectively, above the loose reference line (10).

We have observed the following trends among the dense decorations: the net energies (for a fixed tiling) are found to *decrease* with increasing $x_{\rm Mn}$, and to *increase* with density. Thus DS3.2 is the best and DS2.1 is the worst among dense SI models.

The $x_{\rm Mn}$ trend simply reflects the fact that the ''problem'' sites prefer to be occupied by Mn in structures where they are surrounded mostly by Al neighbors. In these sites, the better option has a site energy roughly 0.5 eV lower than the worse one. The excitation cost should normally be about

twice that difference, and is thus larger than in the loose models.

The density trend indicates that all dense models (even the loosest of them) are packed more densely than optimal, so that the energy can only increase with density. Specifically, it reflects the fact that the ''problem'' sites mostly have rather tight surroundings. It is illuminating to compare the densest ''loose'' model LS.1 and the loosest ''dense'' models DF.1 or DS.3. They have quite similar densities, so the difference is that the dense and loose models achieve this density, respectively, by occupying $\delta$ and $\gamma$ sites; the lower energy of loose models shows that, other things being equal, $\delta$ sites are more costly to fill.

Another trend is that the energies of a series of tilings, with a particular dense SI decoration rule, fall roughly along a straight (tie) line, whereas with a dense FCI decoration they show more scatter. This reflects a quite large ''tile Hamiltonian'' in the dense FCI case. The reason for this may be that in the SI case the resolutions of problem sites are more local, whereas in the FCI case the differentiation of all sites into even/odd flavors forces entanglements of the object types at larger radii.

Not surprisingly, the differences between site energies of the respective orbits show the same trends as in the LS structures. The Mn site energy increases but the Al site energy decreases with the site's radius from the MI center; the orbits with the highest site energies were the ''problem'' sites and the Al sites in the MI.

## VI. RELAXATION OF SIX-DIMENSIONAL MODELS

Plausible quasiperiodic structure models already exist with descriptions that are simple in the standard formulation as a cut through a six-dimensional hypercrystal.[70–72] The CCT atomic models, though simple enough in physical space, would be necessarily complicated to describe in 6D (see paper I, Sec. V). As a test, we have relaxed several well-known quasiperiodic models, under the same potentials,[64] our motivations being:

(i) to check our assumption that the MI is a fundamental motif (the 6D-cut models have lower density of MI's, or no true MI's at all).

(ii) to assess the energy penalty for the simplicity of the 6D-cut description (some rare bad local environments are forced, see Table II in paper I).

(iii) to clarify the relationships between CCT and 6D models (discussed at greater length in paper I).

Our preliminary results suggest that the best 6D models are practically degenerate in energy with CCT decoration models. (Details will be given in Ref. 64.)

We chose three 6D-cut structure models for study (see paper I, Sec. V): the Duneau-Oguey (DO) model,[10] the Katz-Gratias (KG) model,[71,72] and a modified version of the Katz-Gratias model which we called ''KGme.'' For each of those models variants with differing density and chemistry were constructed along the lines of the CCT variants.

The KGme and DO models are built from MI clusters and have FCI and SI space group symmetry, respectively. They have a lower density of MI clusters,[73] but otherwise the local arrangements (and the stability) are similar to the corresponding loose FCI and SI CCT decoration models. For our realistically oscillating potentials (always using $r_{\rm cut}=6.2$ Å) the lowest cohesive energies occurred in (variants of) the DO model. We tentatively associate this with the SI symmetry of that model, since we also found SI symmetry to yield the lowest energies for CCT decorations (see Sec. V and Sec. VIII B). In particular the DO 5/3 approximant was exactly degenerate in energy with our best CCT decoration rule. (We will return to this point in Sec. VIII C.)

The KG model is of interest in this paper mainly in testing whether the 12-atom MI inner shell is necessary for stability and/or low cohesive energies (the *only* difference between KGme and KG is that the KG model has irregular $Al_7$ inner shells). Our preliminary results[64] are unclear, since the energy difference between KGme and KG models depended on the choice of potential truncation. (Note that stability is problematic in the KG models as the 5/3 approximant relaxes to an amorphous state.)

## VII. FURTHER TESTS OF POTENTIALS

In this section, we explore several additional directions in the ''parameter space'' of our calculations, but do so less thoroughly than in the computations of Sec. V; these mostly involve deeper understanding of the role of the potentials. (The crystals and 6D-cut quasicrystals in Secs. III and VI can similarly be considered as exploring additional directions in the parameter space of models.) We start by using molecular dynamics (MD) as a tool to check the stability of various structures (Sec. VII A). Then we focus on separating the effects of the pieces of the potential at different radii. First (Sec. VII B) we study the effects of replacing the ''realistic'' oscillatory potentials by a short-range potential. Next (Sec. VII C) we review the truncation distance effects (obviously important to the robustness of our conclusions), and also (Sec. VII D) compute the contributions to total pair energy from the different wells in $V_{AB}(r)$. Finally (Sec. VII E) we consider the quasilattice constant from the standpoint of our pair-potential analysis.

In most of these supplementary calculations we only used the 3/2-cubic approximant tiling ($T6$ in Table II). This approximant is large enough to contain a variety of different CCT environments but small enough that the relaxation time is not limiting.

### A. Molecular dynamics as a stability test

To test the stability of the decoration models, we performed molecular-dynamics (MD) simulations, using geometries obtained as the output of conjugate gradient relaxations for a group of models. The aim of these simulations is to verify that the system does not get hung up in spurious, shallow local valleys of the structural potential energy. After sufficiently many MD steps, we quench the system and relax the atom positions, and analyze the atomic displacements to see if the initial configuration is recovered.

Our models are listed in Table VIII; they consisted of seven decorations with a representative range of $x_{\rm Mn}$ and atom density, applied to the 3/2-cubic approximant tiling (''$T6$'' in Table II). We adapted the MD code of Roth *et al.*[11] Our typical runs consisted of $2.4\times10^4$ MD steps (each time step corresponds to roughly $3\times10^{-4}$ ps of real time). We performed our analysis (including the quench) not only on

TABLE X. Displacements under molecular dynamics (Å).

| Quantity | $T=0.04$ (loose) | $T=0.04$ (dense) | $T=0.08$ (loose) |
|---|---|---|---|
| Equilibrated: | | | |
| max($\{d_i\}$) | $<\sim 0.5$ | $\sim 0.7$ | 2 – 4[a] |
| median $d_i$ | 0.03 | 0.03 | 0.04 |
| Quenched: | | | |
| max($\{d_i\}$) | $\sim 0.4$ | $\sim 0.7$ | $\sim 5$ |
| median $d_i$ | 0.002 | 0.01 | $\sim 0.02$ |

[a]Depending upon equilibration time.

the final configuration, but also using a configuration taken from halfway through the run. We found no systematic differences between these cases (except as noted below), indicating that our MD run duration is sufficiently long to equilibrate local fluctuations. We used three MD temperatures, $T=0.04$, 0.08, or 0.16 eV (in units where $k_{\text{Boltzmann}}=1$).

The results are summarized in Table X. At $T=0.16$, all the atoms diffuse considerable distances; the system is clearly melted. At $T=0.04$ eV, the configurations are quite stable: in the ''loose'' models, virtually all atoms relax back to their initial positions, within some small distance set by the numerical noise. (In the ''dense'' models, however, the mean displacement is larger, suggesting that many atoms find new stable positions less than 1 Å from their old positions.) At $T=0.08$ eV, the fluctuations are apparently sufficiently anharmonic that our relaxation algorithm fails to converge for most ''dense'' models and for some ''loose'' models. At this temperature, most atoms still relax back to their initial location, but a few of them — the number increases with time — suffer displacements larger than 1 Å. As a rule, if an atom diffuses by as much as 0.3–0.5 Å, its final displacement can be this large (or even larger) after relaxation; on the other hand, atoms which displace about 0.1 Å during the MD run return very nearly to their starting points.

The behavior observed at $T=0.08$ eV suggests that our models have a melting temperature in the vicinity of 0.1 eV$\sim$1000 K, which coincides with the true melting temperature for these materials. The diffusion observed at $T=0.08$ eV is no surprise: the ''loose'' models have many variants which differ only by whether a site is occupied or vacant, so single atoms are expected to diffuse among these nearly degenerate positions.

We also checked the change in ''site energy'' for each atom between the initial and quenched states. This followed the pattern of the atom displacements: i.e., if a few atoms wandered large distances, then a few atoms would gain $\sim 0.4$ eV in energy, however no atom ever takes on unphysically large energies.

In conclusion, our decoration models are stable against finite-temperature molecular-dynamics perturbations. As a side note, our standard criteria about stability (in terms of relaxation behavior) are supported: indeed, those models (loose models) which were more stable under relaxation (compare Secs. II C 3 and V C 1) were also more robust under MD. The rough agreement between the simulated and real melting temperatures of *i*-AlMn adds credibility to the pair potentials we are using.

### B. Short-range potentials

It is interesting to ask whether realistic pair potentials with Friedel oscillations are necessary in order to capture the physics (e.g., to decide which models have a plausible packing of atoms). Many others studying the melting of quasicrystals, or their phonon spectra, have instead adopted toy potentials such as Lennard-Jones[11] (LJ) or Morse[9] potentials which are short range (i.e., have only one minimum).

In prior relaxation studies, a variant of the ''Henley-Elser'' *i*-AlZnMg type model[74] had a robust stability under LJ potentials. On the other hand, the Duneau-Oguey 6D-cut model for *i*-AlMn was found stable under Morse potentials, but the relaxation introduced significant displacive modulations, with a few atoms moving disturbingly far ($\approx 2.8$ Å) in Ref. 9.

To obtain a fair measure of the importance of the Friedel oscillations, we have also carried out relaxations using short-range (specifically Morse) pair potentials on (some of) the same structure models as we relaxed under realistically oscillating potentials. Our Morse potentials have the form

$$V_{ij}^{\text{Morse}}(r)=\epsilon_{ij}\{\exp[-2\alpha_{ij}(r-r_{ij})] - 2\exp[-\alpha_{ij}(r-r_{ij})]\}, \quad (12)$$

where $\epsilon_{ij}$ is the ''depth'' of the minimum, $\alpha_{ij}$ is its ''strength,'' and $r_{ij}$ is position of the minimum (only one well at nearest-neighbor distance); here $i$ and $j$ stand for pairs Al-Al, Al-Mn, or Mn-Mn.

We took $r_{\text{AlAl}}=2.84$ Å, $r_{\text{AlMn}}=2.59$ Å, and $r_{\text{Mn-Mn}}=2.71$ Å to agree with the first minimum of the respective realistic potentials. We set $\alpha_{ij}\equiv 6/r_{ij}$ after Ref. 9, and set $\epsilon_{ij}\equiv 1$, thus fixing a dimensionless energy scale for the Morse potential computations. It should be noted that the depths $\epsilon_{\text{MnMn}}$, $\epsilon_{\text{AlMn}}$, and $\epsilon_{\text{AlAl}}$ in Eq. (12) determine the chemical potentials for Al and Mn, and hence the slope of the fit line in the plot of structural energy versus $x_{\text{Mn}}$. (See Fig. 6.) The truncation cutoff was $r_{\text{cut}}=6.2$ Å (increasing this would have little effect for the Morse potentials).

#### *1. Stability under Morse potentials*

Under Morse potentials, the low-energy crystal structures ''$\alpha$-AlMn'' and $\mu$-AlMn are nearly as stable as under realistic ones, as measured by the sharpness of the PPDF's, and (in ''$\alpha$-AlMn'') and the smallness of the canonical rms. However, the larger CCT approximant models show a more complicated behavior under Morse potentials: the (partial) pair distribution functions (PPDF) remain sharp, as in a stable model; yet the models are unstable by our strict criteria, since more and more individual atoms make large excursions (even 2 Å) from their initial positions, and the canonical rms reaches $\sigma_i\sim 1.2$ Å. for some Al($\gamma_Z$) orbits in the ''5/3'' approximant $T8$.

We can reconcile these conflicting indications of stability and explain the size dependence if we ascribe a large part of these displacements to a strong ''phason-phonon'' coupling in the Morse case. That refers to the elastic displacements which accumulate rapidly with distance as a consequence of phason strain fluctuations[75] (i.e., deviations in the tile distribution from icosahedral symmetry). Thus, in $T8$ the tile nodes themselves are distorted, as seen directly by the ca-

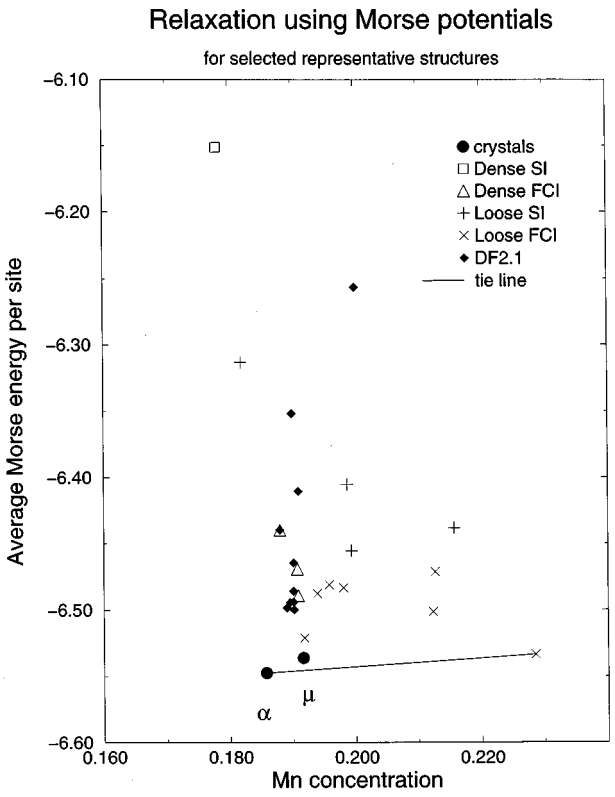


FIG. 6. Energies versus $x_{\mathrm{Mn}}$ as in Fig. 5, but relaxed under Morse potentials. Energies are measured in dimensionless units, roughly comparable to 0.1 eV. Models are identified by a similar key; some 3/2 approximants of 6D-cut structures are included among the models labeled ''loose,'' since they differ from CCT decorations only by the $\gamma_Z(Z_D)$ rings.

nonical rms $\sigma_i \sim 0.17$ Å for the Mn(0) orbit in $T8$; all sites are carried along with the nodes.

This is not, however, the entire story: a smooth distortion should not affect the site energies, yet in the smallish approximant $T5$, the rms variation of site energy is (like the canonical rms) already much larger for *any* orbit under Morse potentials than for the *worst* orbit $[\mathrm{Al}(\beta)]$ under realistic potentials. Furthermore, the Mn-Mn PDF's differ significantly from models relaxed under realistically oscillating potentials and the Mn sites are displaced much farther from the ''ideal'' positions (see Fig. 4). Apparently the rigidity of the Mn subnetwork really depends on the deep second minimum in the realistic Mn-Mn interaction, and perhaps that is what stiffens the entire structure against phason-phonon distortions.

#### *2. Energies under Morse relaxation*

The results of relaxations are shown in Fig. 6. Under the Morse potentials, by far the best models are the crystal phases ''$\alpha$-AlMn'' and $\mu$-AlMn. Among the CCT decoration models the results are more scattered, but it is clear that the FCI models (both loose and dense) are better than the SI models. A comparison on tiling $T6$ of LS1.1 and its loose FCI counterpart, which differ only in the arrangement of the occupied $\delta$ sites, showed the FCI variant had lower energy by 0.030 units. Our interpretation is that, with Morse potentials, a higher occupation of the $\delta$ network $x_\delta \approx 0.50$ is favored, thus forcing an ordering in the lattice gas of $\delta$ sites. (See Sec. VIII B.)

The competition between loose and dense models under Morse potentials depended on two effects.

(i) The parameters $\alpha_i$ in Eq. (12) play an important role since they can change the *shape* of the potential. Potentials with a narrow first-neighbor well match models with a narrow range of first-neighbor distances, as tends to be found in loose models. Dense models have a broader spread of first-neighbor bond radii (especially Al-Al), which is better tolerated by an Al-Al potential with a broader or shallower well.

(ii) Other things being equal, the Morse potentials favor the closest atomic packings.

As a consequence of the competition between (i) and (ii), the loose FCI model (LF) was slightly better than the (densest) dense FCI model DF2.1, when we choose $\alpha_{ij} \equiv 6/r_{ij}$, but the opposite was true after we changed $\alpha_{\mathrm{AlAl}}$ to $4/r_{\mathrm{AlAl}}$.

*Variants.* In contrast to the case of realistic potentials, we found that (i) Al($\gamma_Z$) hexagons in loose SI models are best in the ''6/6'' variant, and (ii) Mn is favored on $\delta_b(A)$ sites while Al is favored on the $\delta_Y$ sites. But just as it was with the realistic potentials, the unphysical filled Mn(0) site is preferred by Morse potentials.

*''Tile Hamiltonian.''* When applying the same rule to different tilings, the tilings under Morse potentials would *not* fall on straight lines in Fig. 6, in contrast to the case of realistic oscillating potentials. By the logic we will present in Sec. IX below, this signifies that the Morse-coupled system cannot be described as a random tiling. The ''tile Hamiltonian'' is rather large in energy (if it can be defined at all). A specific observation was that the energy grew monotonically as a function of the fraction of $D$ cells in the tiling; in the notation of Sec. IX, that means the coefficient $V'_D$ in the ''tile Hamiltonian'' is exceptionally large; physically, it suggests the $D$ cell (in all variants) is rather badly packed for Morse potentials.

### C. Truncation effects

We have just noted (Sec. VII B) that including the potential's oscillations beyond the first-neighbor well makes a real difference in the structure. Further information along the same lines is obtained by comparing the effects of truncating the potential at $r_{\mathrm{cut}} = 11$ Å or a shorter cutoff of $r_{\mathrm{cut}} = 6.2$ Å (see Sec. II C 1). The 6.2 Å cutoff means, roughly, allowing interactions to the second or third shell of neighbors. This tests the validity of our entire program of relaxations since: (i) due to relaxation time limitations we used the shortened cutoff for most of the calculations reported here, assuming that this would have only minor effects on the answers; (ii) if $r_{\mathrm{cut}} = 11$ Å gives answers different from $r_{\mathrm{cut}} = 6.2$ Å, then the oscillating tails of the potentials are still important at these radii, hence using an even longer cutoff might give yet another answer.

The principal artifact of the 6.2 Å cutoff among loose models is in a wrong sign of the *energies* resulting from the $\delta_Y$ site occupancy by Al, Mn, or a vacancy. This must be blamed on the omission of the *third* minimum of the potential $V_{\mathrm{MnMn}}(r)$, at about 6.7 Å (see Fig. 1); indeed, the re-

TABLE XI. Structural energy by wells (in eV/atom).

| Model[a] | $x_{\mathrm{Mn}}$ | $E^{(1)}$ | $E^{(2)}$ | $E^{(3)}$ | $E_{\mathrm{tot}}$ |
|---|---|---|---|---|---|
| LS1.1 | 0.1993 | -0.0238 | -0.2083 | 0.0423 | -0.1898 |
| DF2.2 | 0.2079 | -0.0235 | -0.1782 | 0.0433 | -0.1584 |

[a]Tiling $T6$ was used.

laxed Mn-Mn pair-distribution function has a peak around 6.7 Å which includes contributions from Mn($\delta$) atoms. Dense models seemed to fit *worse* with potentials using $r_{\mathrm{cut}}=11$ Å than with $r_{\mathrm{cut}}=6.2$ Å, as seen not only in failure of certain models to satisfy our stability criteria for relaxation, but also in higher ''canonical rms'' values after successful relaxations.

### D. Allocating energy by wells

To obtain further understanding of the relationship between models and potentials, we separated the contributions from the first-, second-, and third-neighbor wells in each pair potential. That is, for each of the three potentials in Fig. 1, we let $r_j$ be the radius of the $j$th maximum ($r_0\equiv 0$), then all contributions from the interval $(r_{j-1},r_j)$ were allocated to the $j$th well.

This analysis confirmed that what favors loose models over dense ones is the contribution from the *second* wells (of all three potentials). For a striking example, we compare the densest dense model (DF2.2) to one of the loose models (LS1.1); these have similar $x_{\mathrm{Mn}}$ values of 0.2079 and 0.1993, respectively. The pair energy contributions from the first and third wells are about the same, but the second wells of the oscillating potentials favor the loose model by 0.03 eV/atom.

This conclusion fits reasonably well with the finding that models with ''pseudovacancies'' are not stabilized by Morse potentials (Sec. VII B). After all, if we had truncated our potentials after the first well, we would have created a short-range potential qualitatively similar to Morse potentials (although dramatically different in the ratios of the well depths). The results are shown in Table XI.

### E. Quasilattice constant

We have explored the effects of varying $a_q$. (This could just as well be viewed as varying the radii of wells in the potential, if we consider $a_q$ as fixed.) We computed the relaxed energies (using $r_{\mathrm{cut}}=6.2$ Å), for the four best loose decoration rules (LS1.1, LS2.1, LS2.4, and LS3.1) on tiling $T6$, varying $a_q$ by 0.01 Å increments. There is a (quadratic) minimum of the relaxed energy $E(a_q)$ near 4.60 Å for the ''best'' rule LS3.1 (at 4.61 or 4.62 Å for the other rules).

These experiments with $a_q$ address the first of the worries about pair potentials in Sec. II B. Instead of choosing $a_q=4.60$ Å throughout, as we have in all other sections, a more physical rule would be either to force the right conduction-electron density for our potentials, $\rho_{\mathrm{el}}=\rho_0$, or perhaps to adjust $a_q$ so as to optimize our structural energy. The above-mentioned results show that either choice would have a very small effect on our results; e.g., had we optimized $a_q$ for each decoration, it would have lowered the energy by only 0.001 meV/atom, which is much smaller than the differences between the different decoration rules.

These results are also relevant to the second worry in Sec. II B. Properly speaking, we should include the structure-independent contribution $U_0(a_q)$, and then should minimize the sum $U_0(a_q)+E(a_q)$, in order to determine the relaxed energy for a given topological arrangement of atoms;[76] obviously the whole curve $E(a_q)$ would be needed for such a calculation.

## VIII. DISCUSSION OF STRUCTURAL TRENDS

In the spirit of Sec. II D, we now try to make sense of our results in terms of the distinctive features of the structures and the potentials. The unifying theme of our discussion is the $\delta$ site occupations, in particular the negative vacancy formation energies (favoring ''pseudovacancies'') possible on many of them. This is why loose SI structures are favored, and why (see Sec. IX) the tile Hamiltonian is small.

The possibility that the vacancy formation energies are wrong, owing to the weak aspects of our potentials (Sec. II B), is a cause for some concern. However, the arguments in this section could be inverted as follows. It would seem that good behavior in a quasicrystal model is conditioned on the ''looseness;'' thus, we would speculate that the high-quality quasicrystals such as $i$-AlPdMn must have loose-type structures, even if the best structure of real $i$-AlMn is not loose. (We suspect that a better calculation would bear out the general pattern of pseudovacancies on the $\delta$ sites, but perhaps not on the *same* $\delta$ sites are found in the present paper, since this can be sensitive to potential tails and other small energy differences.) In any case, the ''looseness'' has emerged more clearly as an essential parameter for discussing Al-TM models.

### A. Why are loose structures favored?

The key to this point is the discussion of the candidate $\delta$ sites in Sec. IV D of paper I. The $\delta$ atoms were viewed as a lattice gas on this network, and the loose and dense model families were primarily distinguished by the minimum spacing $r_\delta$ among these atoms. It was argued that the ideal occupancy of this network $x_\delta$ is less than 50%.

We propose that the optimal value of $x_\delta$ is $\sim 0.33$ (as in a typical loose model); and that, so long as the indirect exclusion is satisfied, it does not matter very much exactly where those occupied $\delta$'s are distributed: the lattice gas really looks like a gas. Our claim that the placement of the $\delta$ atoms does not matter much is reflected in our finding — see Sec. V — that on such sites the competition between variant occupations by Al, Mn, or (pseudo)vacancy is very delicate.[77]

Diffraction experiments indicate AlMn (like all other Al-TM quasicrystals) does have nonzero occupancy of $\delta$ positions.[78] Our finding that, among loose models, LS2 structures are preferred over the LS3 structures is thus in accord with experiment. It is only using potentials truncated at $r_{\mathrm{cut}}-6.2$ Å that the extreme loose structure LS3 (which has *no* occupied $\delta$ sites) is preferred, presumably a spurious effect.

### B. Why is there SI symmetry?

Our finding that SI models are preferred ran counter to our *a priori* expectation that FCI structures would be favored [based on $\alpha$-AlMnSi (Ref. 79) and $i$-AlCuFe]. The lack of ordering can be interpreted in light of the above viewpoint of the $\delta$ sites as a lattice gas, within a surrounding that has SI order. If the net occupation of $\delta$ sites is low, as in a loose model, then their mutual interactions are unimportant and the single-site terms determine the structure. Thus it will be SI.

From the above arguments, we would have conjectured that an FCI ordering should be favorable for dense models, since it is the best solution to the repulsive $\delta$-$\delta$ interactions. However, numerically SI was found to win also in the dense case. Apparently the single-site terms favoring certain subclasses of $\delta$ sites outweigh the $\delta$-$\delta$ interactions, even in this case.

### C. Why Mackay icosahedra?

In our CCT decoration models, we assumed that MI clusters were fundamental in two senses:

(i) we have complete MI clusters rather than fragmentary or imperfect ones,

(ii) the number density $n_{\mathrm{MI}}$ of MI should be as high as possible.

This point is somewhat controversial, as $i$-AlMnSi diffraction data was interpreted in favor of pseudo-MI rather than MI clusters,[67] but it is now understood that even good data may be insufficient to decide the question.[80]

Assumption (ii) can be addressed by a systematic comparison of relaxed energies including both CCT-decoration and 6D-cut models, since all of the latter contain a lower density of MI's than in a CCT structure. Calculations of this sort are in progress.[64] A related kind of structure that might also be compared is a decoration model based on a generalized CCT (using some larger types of canonical cell, and thus permitting lower MI number densities).

Assumption (i) is also addressed appropriately via the 6D models, since they contain fragmentary MI's wherever a complete MI could not be placed on a candidate MI centers, due to overlap with another MI separated by a short distance $a_q$, and some of them contain pseudo-MI's in place of MI's.

It seems unlikely that MI's should be imperfect in the second shell, which has a packing that can hardly be improved by a rearrangement. On the other hand, for all of our good decoration rules, the MI first shell sites [$\alpha$(Al)] have the worst site energies of any Al orbit [about 0.01 eV worse than Al($\beta$) or Al($\gamma$) in loose models].[81] This suggests this shell ought to be modified, perhaps by making two $\alpha$ sites vacant in each MI. This option might also be studied in a 6D representation, where it appears as a compromise between the MI $Al_{12}$ shell and the pseudo-MI $Al_7$ shell.

To rule out MI fragments, we would have to explore an even larger space of possible structures. For example, they might be based on motifs such as $Al_6Mn_4$ tetrahedra and ''pentagonal bipyramid'' clusters, which are, respectively, like 1/20 or 5/20 fragments of an MI.[82,38] Finally, we observe that the two-shell mini-Bergman clusters are conceivably just as important (for the cohesive energy) as the three-shell MI clusters.[83]

### D. Mn stoichiometry

Experimentally, $i$-AlMn seems to have highest quality around $x_{\mathrm{Mn}} \approx 0.20$, but it admits a range from about 0.14 to 0.22. Our results from loose models would indeed predict a wide range of $x_{\mathrm{Mn}}$ values: the fact that the energies cluster along a straight (not curved) line in Fig. 5 shows that different stoichiometries are equally acceptable. There are two contributing reasons, in terms of tile and site disorder, respectively.

One reason for the wide range in our models is that $D$ cells tend to be much richer in Mn than $A$ cells — for rule LS3.1, the $x_{\mathrm{Mn}}$ is roughly 0.24 for the $D$ cell and 0.19 for the $A$ cell. The causes of this are that (i) the optimum occupation of the $\delta_b$ sites in $A$ cells is a (pseudo)vacancy, while the $\delta_Y(D)$ site is reasonable as a Mn; (ii) the $D$ cell has the highest density of Mn($\nu$) and Mn($\mu$) sites. In turn, canonical-cell tilings can have varying fractions of $D$ versus $A$ cells (obvious in simple structures built from only one kind of tile; but even with icosahedral symmetry, there is considerable freedom in these fractions[8,55]).

An independent reason for variable stoichiometry is that the loose models contain many $\gamma_{3D}$ and $\delta$ sites on which Mn or Al are almost equally good, so that the real structure may have a stochastic occupation implying a phase with variable concentration.

## IX. TILE HAMILTONIAN RESULTS

The decoration description of a quasicrystal may permit us to describe the energetics in terms of a reduced set of degrees of freedom. Indeed, we have seen (Sec. V) that the ''canonical rms'' of the *relaxed* positions is small. That means that the atomic coordinates are well described by a configuration of rigid tiles plus as subsequent decoration in which tiles of a given kind receive identical configurations of atoms. It was argued (cf. paper I, Sec. VI) that such a lack of ''context sensitivity'' may permit us to account for the structural energies in terms of a ''tile Hamiltonian'' $\mathscr{H}_{\mathrm{tile}}$, a model Hamiltonian which assigns just one degree of freedom per tile.[84] The fact that energies from many different tilings fall nearly on a straight tie line (in Fig. 5) confirms, at least, that tile rearrangements are valid low-energy excitations. However, to say that the tile Hamiltonian description is valid, the deviations from the straight line behavior must not only be small, but their values should be mostly accounted for by $\mathscr{H}_{\mathrm{tile}}$. In this section, we shall extract the parameters in $\mathscr{H}_{\mathrm{tile}}$, using as input the relaxed energies presented above (Sec. V), and confirm that the ''tile Hamiltonian'' description is rather accurate. (This works only for the loose decoration models under realistic potentials.)

We consider the simplest possible form

$$\mathscr{H}_{\mathrm{tile}} = \sum_{\alpha} V_{\alpha} N_{\alpha}, \tag{13}$$

which includes *only* one-tile terms, as in Eq. (2) from paper I, where $\alpha = A,B,D,E$ for four kinds of tile. (We do not have an independent $V_C$ since $N_C \equiv N_B + 2N_E$; thus $V_B$ represents the sum of $B+C$ tiles and $V_E$ represents $E+2C$.) We assume the validity of Eq. (13), equate $\mathscr{H}_{\mathrm{tile}}$ to the relaxed energies for tilings $T1$, $T2$, $T3$, and $T4$, and so find $\{V_\alpha\}$ as

TABLE XII. Tile Hamiltonian results.

| Rule | $r_{\rm cut}$(Å) | $\tilde{\mu}_{\rm Al}$ | $\tilde{\mu}_{\rm Mn}$ | $V'_\alpha/N_\alpha$ (meV/atom) $A$ | $B$ | $D$ | $E$ |
|---|---|---|---|---|---|---|---|
| LS3.1 | 6.2 | 368 | -2455 | -0.633 | -2.011 | 0.462 | 1.930 |
| LS1.2 | 6.2 | 304 | -2179 | -2.212 | 2.623 | -2.415 | 3.883 |
| LS1.2 | 11.0 | 365 | -2687 | 1.780 | -2.540 | 0.759 | 1.970 |
| LS2.4 | 11.0 | 379 | -2744 | 1.150 | -4.130 | 0.489 | 3.240 |
| DF2.1[a] | 6.2 | -1015 | 930 | -0.908 | 5.967 | 0.403 | 10.551 |

[a]Under Morse potentials, and modified DF2.1 decoration rule. In $10^{-2}$ Morse units.

the solution of the four linear equations Eq. (13) with the $N_\alpha$ values for those tilings as coefficients. Of course, the validity of this description must be tested by checking Eq. (13) for a variety of other tilings.

#### Results for "tile Hamiltonian"

We first find the parameters $\tilde{\mu}_{\rm Al,Mn}$ (for each decoration rule) by a least-squares fit of the relaxed energy/atom (weighted equally for each of the 11 example tilings) to

$$E_{\rm rel}=\tilde{\mu}_{\rm Al}(1-x_{\rm Mn})+\tilde{\mu}_{\rm Mn}x_{\rm Mn}. \tag{14}$$

Then as explained in paper I, the parameters meaningful for comparative structural stability are obtained by subtracting off the line of Eq. (14):

$$V'_\alpha=V_\alpha-\tilde{\mu}_{\rm Al}N_\alpha^{\rm Al}-\tilde{\mu}_{\rm Mn}N_\alpha^{\rm Mn}, \tag{15}$$

where $N^{\rm Al,Mn}$ is the number of Al,Mn atoms on a tile of type $\alpha$. Note that in principle the subtracted parameters $\{V'_\alpha\}$ are linearly dependent — there are really only two independent parameters among them.

For selected combinations of decoration rules and potentials, Table XII shows the subtracted tile energy per atom, for each kind of tile.[85] Then Table XIII shows the difference $E_{\rm rel}-\mathscr{H}_{\rm tile}$ when the parameters in Table XII are inserted into Eq. (15) for tilings $T5-T11$ from Table II. (Of course, this is zero by construction for tilings $T1-T4$.)

The $V'_\alpha$ values in Table XII are of order 1 meV. That is about ten times bigger than the residuals $\mathscr{H}_{\rm tile}-E_{\rm rel}$ which are typically $\sim\pm0.15$ meV/atom (see Table XIII). This confirms that our simple tiling Hamiltonian is a good approximation. Presumably, much of these residuals could in turn be accounted by including tile-tile interactions in Eq. (15).

Note in Table XIII that the residuals are smaller with the reduced cutoff $r_{\rm cut}=6.2$ Å than with $r_{\rm cut}=11$ Å. This presumably reflects the omission of many direct interactions of further neighbor atoms in two neighboring tiles – $r_c=6.2$ Å is less than a tile diameter.[86] When we reduce the interaction radius even further (by using Morse potentials), it appears that the residuals (Table XII) become smaller, relative to the energy scale set by the one-tile terms (Table XIII). In the absence of longer-range interactions, the residual tile-tile interactions may be ascribed to elastic distortions — i.e., interactions between atoms on different tiles are mediated by pushing on the intervening atoms.[86,87]

The values of $V'_\alpha$ are very small compared to other energy scales — e.g., they are $\sim1/100$ times the excitation cost of the higher-energy alternative occupancy in the "problem" sites, an energy difference which was considered small (see Sec. V A 2). Thus it is fair to say that a "random tiling" is appropriate as a first-order approximation for *i*-AlMn. The smallness of the $\mathscr{H}_{\rm tile}$ is a consequence of "looseness" (see Sec. VIII A). In a dense model, atoms in different tiles are pressed up against each other and so they interact more strongly giving a much larger $V'_\alpha$.

We now consider whether the deviations from degeneracy are small enough to permit "entropic stabilization"[4] of an equilibrium quasicrystal. In the Al-Mn system, this possibility is ruled out since some crystalline states were found lower in energy than the CCT states (in accord with the fact that real *i*-AlMn is only metastable). Instead let us consider a hypothetical system in which all the CCT packings are lower in energy than other structures, but the energy differences among CCT structures are similar to those found here for the AlMn case (it is plausible that *i*-AlPdMn would fit this desciption).

The energy scale $\bar{V}$ of our "tile Hamiltonian" (Table XII) is $\sim1$ meV/atom or $\sim$ 70 meV ($\approx$800 K) per CCT node. Furthermore, the CCT random-tiling entropy is at most $\sigma_0\approx0.1$ per node.[88] Now, a quasicrystal is *entropically stabilized* when $\sigma_0 T>\bar{V}$, i.e., above $\sim10^4$ K using the parameters for random-tiling *i*-AlMn. Since the real melting temperature is $T_m\simeq10^3$ K, entropic stabilization cannot be realized, unless $\bar{V}$ is reduced by an order of magnitude.

## X. CONCLUSION

This paper demonstrates the use of detailed energetic studies as the basis for structural insight and refinement for the case of Al-Mn as modeled using canonical-cell tilings. Though our results center on the Al-Mn system, they reflect a more general philosophy which advocates a synthesis of diffraction studies with total energy methods in the refine-

TABLE XIII. Error in $\mathscr{H}_{\rm tile}$ (meV/atom).

| Rule | $r_{\rm cut}$(Å) | $T5$ | $T6$ | $T7$ | $T8$ | $T9$ | $T10$ | $T11$ |
|---|---|---|---|---|---|---|---|---|
| LS3.1 | 6.2 | 0.21 | -0.06 | -0.07 | -0.19 | -0.00 | -0.06 | 0.04 |
| LS1.2 | 6.2 | -0.79 | -0.37 | -0.60 | -0.38 | -0.47 | -0.42 | -0.60 |
| LS1.2 | 11.0 | -2.58 | -0.98 | -0.85 | -0.97 | -1.33 | -1.04 | -1.40 |
| LS2.2 | 6.2 | -0.79 | -0.06 | -0.13 | -0.44 | -0.32 | -0.22 | -0.32 |
| LS2.4 | 11.0 | -2.58 | -0.27 | -0.42 | -0.74 | -1.00 | -0.65 | -1.12 |
| DF2.1[a] | 6.2 | 0.42 | -8.14 | -7.53 | -5.28 | -6.92 | -6.99 | -6.48 |

[a]Under Morse potentials, and modified DF2.1 decoration rule. In $10^{-2}$ Morse units.

ment of quasicrystal structures.

Our approach has been to use pair potentials which simultaneously treat both the free-electron and tightly bound electronic degrees of freedom. These potentials exhibit strong Friedel oscillations which favor particular interatomic spacings that favor complex intermetallics. Our results from applying these potentials to structure refinement in the Al-Mn system are summarized below, followed by suggestions for future work along these lines.

### A. Summary of the results

We have systematically explored the energetics and stability of many different structural models based on canonical-cell tilings, assuming pair potentials, in order to grasp the relationship of particular features in the structure to the resulting total energy. Within the families of models we studied, the most important kind of variation was of site occupancy — above all, the competition between filling the site or making it vacant (''density variations''). It is much easier technically to modify such details in the tiling-decoration approach than in the 6D approach, where one must first encode it as a context dependence and then must figure out what acceptance domain corresponds to that context. The generally good match between the pair potentials and known Al-Mn structural patterns indicates that structure refinements in quasicrystals could quite practically incorporate realistic energy calculations to resolve uncertain details.

All of our quasicrystal models still lie above the tie line of the best real structures, and hence are predicted to be thermodynamically unstable (at $T=0$), just like real $i$-AlMn; however, our models are competitive with several plausible small crystal structures which are also unstable for Al-Mn (see Sec. III). As to our further finding that the best quasicrystal has SI order, experiment is ambiguous in that $i$-AlMn is SI, but short-range FCI order may appear upon annealing.[79]

In the past, optimal packing of atoms as in sphere packings,[89] guided by information from crystallographic refinements, has been a mainstay in constructing possible quasicrystal decorations.[13,90] But our results in this paper show that packing is *not* a good guide for guessing the details of Al-Mn structures; for these details depend sensitively on the oscillating, further-neighbor tails of the interatomic potentials. Under realistically oscillating potentials, those well-packed structures appear *overpacked*; the loose models were favored instead. On the other hand, short-range potentials with one well, such as the Morse potential, *do* favor the well-packed type of structure; indeed the more realistic loose structures tend to be unstable when relaxed under Morse potentials. It is vital to adopt the most realistic possible form of potential.

The loose models, taken together, demonstrate that the description of atomic sites by ''canonical orbits'' is unexpectedly accurate, capturing the post-relaxation positions of the atoms to within $\sim 0.1$ Å (see the entries $\bar{\sigma}$ in Table VI), without excessively many parameters. Presuming that the *true* positions can be captured as easily, this is encouraging for possible future diffraction refinements of CCT decoration models. Another consequence of this fact is that the energy costs for tile rearrangements (also known as phason fluctuations) are quite small. Thus, there may exist a simple additive ''tile Hamiltonian'' (Sec. IX) from which we could calculate that energy cost, for any given tiling. These calculations are an explicit implementation of the idea of building an effective model with parameters determined by calculations at smaller length scales and raise the possibility of simulations at the tiling level based upon microscopically derived Hamiltonians.

We have explored, more systematically than in any prior work, some of the many directions in the parameter space of our calculation, which concern the model (variations of density $\rho_{\rm at}$ or stoichiometry $x_{\rm Mn}$ and SI/FCI symmetry) as well as the potentials (range/truncation, lattice parameter). Yet our studies are still incomplete at many points. For example, it is surely confirmed that the Mackay icosahedron (MI) cluster is a possible structural motif, but we could not really settle its importance since we did not explore a sufficient variety of models with fewer (or none) of the MI's (see Sec. VIII C).

There are a few other areas in which our results are not entirely satisfactory. Our finding that the best version of $\alpha$ phase has filled MI centers certainly contradicts the known structure of $\alpha$-AlMnSi. This may be an artifact of replacing Si by Al in our model; more likely, it is an artifact of using additive pair potentials at the MI center (where, e.g., ''glue'' potentials can account for the pseudovacancy[33]).

More fundamentally, our pair potential scheme has limitations: we cannot escape the fact that the available potentials are calculated only for electron density $\rho_0$ (see Sec. II B). and are unreliable for Mn-Mn neighbor pairs. In particular, our conclusion that relatively low density and SI symmetry are favored depends crucially on the sign of the vacancy formation energies for certain sites known as ''$\delta$'' sites, or equivalently six-dimensional body-center sites; see Sec. VIII and paper I, Sec. IV D . Since we do not know how robust the vacancy formation energies are, it is quite likely that a better set of potentials will change our conclusions in Sec. V as to the detailed ranking of models. Indeed, the physically correct answer may depend sensitively on small details of the second-neighbor potential wells and vacancy formation energies, which will be a function of composition. Further discussions of the results are found in Sec. VIII. However, despite all the uncertainties, we believe that our finding in favor of loose structures is robust, because it is a necessary condition for the existence of a good tiling description (see Sec. IX).

### B. Future directions

Our results might serve as the prototype for an analogous calculation for the more interesting stable ternary quasicrystals, $i$-AlPdMn and $i$-AlCuFe. In view of the experimental facts, we would expect find the FCI quasicrystal lower in energy than the competing crystal (or SI quasicrystal) phases. On the nearest-neighbor scale, these ternaries surely have atomic patterns similar to those in the models studied here, and a structure model may well be based on variants built on the structure models of paper I. (This assumes that $i$-AlPdMn contains no MI clusters, which is a controversial point, but may well be consistent with diffraction.[80]) Al-TM ternary calculations are not presently feasible since effective pair potentials have not yet been calculated for the ternaries,[91,92] except in the $i$-AlCuLi family[17] which is more tractable, as noted in Sec. II.

Such a calculation might be able to settle the controversy about the importance of entropic stabilization (see Ref. 8) for the stable, long-range-ordered quasicrystals. In Sec. IX, we estimated that our model *i*-AlMn would be stabilized, relative to a phase-separated mix of CCT approximants, at temperatures above $\sim 10^4$ K. Such a phase would be unstable first because a phase-separated mix of small crystal structures has a lower cohesive energy in the Al-Mn case, and second because the melting temperature is $10^3$ K. But it would not be surprising if in some other alloy system (perhaps *i*-AlPdMn) the CCT arrangements may be favored energetically over the non-CCT small crystal structures. If we can also reduce the scale of the tile Hamiltonian $\bar{V}$ by an order of magnitude, an entropically stabilized quasicrystal phase will exist in a temperature range above $\sim 10^3$ K, i.e., may persist in some window below $T_m$ as the stable equilibrium phase. It is easy to imagine doing this by fine tuning the potentials and the decoration.[93] If, furthermore, the tile Hamiltonian could be accurately evaluated, this would open the door to Monte Carlo simulations in which (only) the tiling was rearranged, for the purpose of (i) measuring the phason elastic constants[5,88] or (ii) discovering the absolute ground-state tiling of the model, to test whether or not it is ideally quasiperiodic.

Kinetic calculations, similarly relating to high-temperature (i.e., realistic) properties, can also be based on our energy results. These would be particularly interesting if performed for the case of a *stable* quasicrystal such as *i*-AlPdMn. For example, the conclusion of paper I noted the desirability of understanding the atomic rearrangements induced by tile rearrangements (a purely geometrical question). Along with that it is natural to determine the energy barriers along the optimal paths of those rearrangements. The barriers would determine the kinetics permitting the relaxation of phason strain at elevated temperatures.

The smallness of the tile Hamiltonian in our calculations was a consequence of the looseness of our *i*-AlMn models. In the light of the preceding discussion on tile kinetics, we can turn this observation around: good quasicrystals allow phason relaxation on human time scales, and this is possible only if the tile Hamiltonian is small (whether or not it implements matching rules for quasiperiodicity). Thus we conjecture that *i*-AlCuFe and *i*-AlPdMn probably have loose-type structures. (Indeed, the popular Katz-Gratias 6D-cut model for these alloys *is* a loose structure; see Sec. VI.)

In addition to tile disorder, site disorder (important both for statics and dynamics) is also illuminated by our calculations. In our *i*-AlMn models at least, we expect site disorder to be prominent on the $\delta$ sites. At high temperatures, the entropy of atoms occupying the $\delta$ network could be sizable, and could easily be larger than the random-tiling entropy due to the different (almost degenerate) configurations of cluster centers.[96] One would also expect *diffusion* to occur most easily via the $\delta$ network.[95] In *i*-AlCuFe, Mössbauer spectroscopy[94] showed hopping by Cu atoms by distances $\sim 4$ Å; this could easily be ascribed to the $\delta$ network, since Cu sits preferentially on the $\delta$ sites[71,72] and $a_q \approx 4.5$ Å is the shortest distance between candidate $\delta$ sites.

## ACKNOWLEDGMENTS

This work has been supported by DOE Grant No. DE-FG02-89ER45405. We are grateful to M. Krajči for the use of his relaxation code, to J. Roth for the use of his molecular-dynamics code, to M. E. J. Newman for help with the approximants from Ref. 54, and especially to J. Zou, A. Carlsson, and M. Widom for their help in the construction of potentials. We also thank M. Oxborrow for collaboration in earlier stages and E. Cockayne for comments on the manuscript.

## APPENDIX A: EXPLANATIONS OF TYPICAL MOTIFS

In this appendix, we review the rationalizations of the observed typical local patterns (see Sec. III A in paper I) in terms of the oscillating potentials depicted in Fig. 1. A tendency to uniform spacing of Mn atoms is partly explained by the shape of the potentials.[19] Since there is no first-neighbor well, Al-Al nearest neighbors are strongly disfavored (yet they are inevitable, since most of the atoms are Al). This provides the first reason why Mn-Mn not only avoid nearest neighbors, but also are spaced uniformly: such an arrangement maximizes the number of Al-Mn neighbors, hence minimizes the number of Al-Al neighbors, as explained in Ref. 14 in the similar case of Al-Co. A secondary reason for the uniform spacing is the strong second minimum in the Mn-Mn potential at around 4.7 Å.[14]

The $Al_3Mn$ tetrahedra are favored by the strong Al-Mn nearest-neighbor attraction, which favors local close packing. Twenty such tetrahedra constitute the very common $Al_{12}Mn$ icosahedron motif (Ref. 33 gives another approach to explaining the $Al_{12}Mn$ icosahedra). In turn, the MI cluster is a super-icosahedron of $Al_{12}Mn$ icosahedra.[33]

The existence of holes (in particular the ''pseudovacancies'') in the structure becomes more plausible after reviewing the potentials, if we recollect that there is no significant nearest-neighbor Al-Al attraction. Consider, for example, an empty Al icosahedron: its radius should be set so that the second-neighbor bond lengths are satisfied, but then the remaining hole is just a little too small to fit another Al atom. The sign of the energy change upon filling such a hypothetical site with an atom might be dependent on distant neighbors.

*Present and permanent address: Institute of Physics, Slovak Academy of Sciences, Dubravska cesta 8, 842 28 Bratislava, Slovakia.

[1] S.-J. Poon, Adv. Phys. **41**, 303 (1992).

[2] C. Sire, in *Lectures on Quasicrystals*, edited by F. Hippert and D. Gratias (Les Editions de Physique, Les Ulis, France, 1994), p. 505.

[3] C. Berger, in *Lectures on Quasicrystals* (Ref. 2), p. 463.

[4] C. L. Henley, in *Quasicrystals and Incommensurate Structures in Condensed Matter*, edited by M. J. Yacaman, D. Romeu, V.

Castaño, and A. Gómez (World Scientific, Singapore, 1990), p. 152; M. Widom, in *Quasicrystals*, edited by M. V. Jarić and S. Lundqvist (World Scientific, Singapore, 1990), p. 337.

[5] C. L. Henley, in *Quasicrystals: the State of the Art*, edited by P. J. Steinhardt and D. P. DiVincenzo (World Scientific, Singapore, (1991), p. 429.

[6] M. Mihalkovič, W.-J. Zhu, C. L. Henley, and M. Oxborrow, preceding paper, Phys. Rev. B **53**, 9002 (1996). Brief preliminary reports of our work have appeared in M. Mihlakovič, W.-J. Zhu, C. L. Henley, M. E. J. Newman, M. Oxborrow, and R. B. Phillips, in *Aperiodic '94*, edited by G. Chapuis and W. Paciorek (World Scientific, Singapore, 1995), p. 169; and W.-J. Zhu, C. L. Henley, and M. Mihalkovič, in *Proceedings of ICQ5*, edited by J.-M. Dubois (World Scientific, Singapore, in press).

[7] V. Elser and C. L. Henley, Phys. Rev. Lett. **55**, 2883 (1985).

[8] C. L. Henley, Phys. Rev. B **43**, 993 (1991).

[9] F. Lançon and L. Billard, J. Phys. (Paris) **51**, 1099 (1990).

[10] M. Duneau and C. Oguey, J. Phys. (Paris) **50**, 135 (1989).

[11] J. Roth, J. Stadler, R. Schilling, and H.-R. Trebin, J. Non-Cryst. Solids **153**, 536 (1993).

[12] M. Krajči and J. Hafner, Phys. Rev. B **46**, 10669 (1992).

[13] M. Oxborrow, Ph.D. thesis, Cornell University, Ithaca, 1993.

[14] R. Phillips, J. Zou, A. E. Carlsson, and M. Widom, Phys. Rev. B **49**, 9322 (1994).

[15] M. Widom, J. Zou, and R. Phillips, Philos. Mag. A **71**, 397 (1995).

[16] I Štich, M. C. Payne, R. D. King-Smith, J. S. Lin, and L. J. Clarke, Phys. Rev. Lett. **68**, 1351 (1992); K. D. Brommier, M. Needels, B. E. Larson, and J. D. Joannopoulos, *ibid.* **68**, 1355 (1992).

[17] M. Windisch, J. Hafner, M. Krajči, and M. Mihalkovič, Phys. Rev. B **49**, 8701 (1994). They have derived true ternary Al-Cu-Li potentials using pseudopotential perturbation theory and including Cu *d* orbitals in a tight-binding approximation. However, for relaxation they adopted (Al,Cu)-Li pseudobinary potentials, to conform to the chemical disorder reported by diffraction refinements.

[18] R. Phillips and A. E. Carlsson, Phys. Rev. B **42**, 3345 (1990); R. Phillips, H. Deng, A. E. Carlsson, and J. S. Daw, Phys. Rev. Lett. **67**, 3128 (1991).

[19] J. Zou and A. E. Carlsson, Phys. Rev. B **47**, 2961 (1993).

[20] J. Zou and A. E. Carlsson, Phys. Rev. Lett. **70**, 3748 (1993).

[21] A. E. Carlsson, J. Zou, and R. Phillips, in *Alloy Modeling and Design*, edited by G. M. Stocks and P. E. A. Turchi (The Minerals, Metals, and Materials Society, Warrendale, PA, 1994), p. 13.

[22] Another approach was to construct oscillating potentials from the pair-distribution function, whose oscillations have no necessary relationship to the Friedel oscillations or to the real structural energy differences; see Ref. 11.

[23] J. Zou (unpublished).

[24] J. Friedel, Philos. Mag. B **65**, 1125 (1992).

[25] G. Trambly de Laissardière, D. Mayou, and D. Ng. Manh, Europhys. Lett. **21**, 25 (1993).

[26] Even if our valence (and hence our $k_F$) were wrong, we suspect that the fit to the *ab initio* results on fcc $Al_3Mn$ would also shift $\phi$ in Eq. (5) that the *second* potential well would be close to correct. Then our results would still be meaningful, since (see Secs. VII and VIII) they are sensitive mainly to the second well.

[27] It would be just as easy to compute the potentials for any other value of $\rho_{\rm el}$, but it would be computationally demanding to cover a large number of values. The Al-Co potentials in Ref. 14 were computed at several electron densities.

[28] For the relaxations in Ref. 13, the dimensions of the unit cell were adjusted so as to force the electron density to be the value assumed for our calculations.

[29] K. Yu-Zhang, Thèse de Doctorat de l'Universite de Paris VI, Paris, France, 1988, p. 31.

[30] N. W. Ashcroft and D. Stroud, in *Solid State Physics: Advances in Research and Applications*, edited by H. Ehrenreich, F. Seitz, and D. Turnbull (Academic, New York, 1978), Vol. 33.

[31] In *i*-TiMn, direct *d*-*d* hopping produced strong three- and four-atom effective interactions; see Ref. 18.

[32] This uncertainty on the treatment of vacancies clouds many of our important results, since they depend on the negative vacancy formation in certain sites.

[33] A. Redfield and A. Zangwill, Phys. Rev. Lett. **58**, 2322 (1987); Philos. Mag. Lett. **57**, 255 (1988).

[34] To be precise, we have used 10 Å for some data sets, but we believe there is no significant difference from "11 Å."

[35] For the relaxations of small crystal structures (Sec. III) and of structures annealed using molecular dynamics (Sec. VII A) we used a different code, due to M. Krajči, which does not take advantage of the symmetries; it uses a generalization of the conjugate-gradient method, and has a similar stopping criterion. When both codes were used on the same structure, the results were very nearly the same.

[36] In order to relax efficiently the very large cubic structures, we have used the net-cube algorithm for fast updating of pair distances information.

[37] There are also closely related but smaller "holes," where the surrounding atoms are just a bit too close to permit an atom.

[38] At the time of our calculations, we were unaware of the recent solution of the $\lambda$-$Al_{80}Mn_{20}$ structure by G. Kreiner and H. F. Franzen, J. Alloys Compounds **221**, 15 (1995). That work also discusses at length structural motifs, similar to those we outlined in Sec. II D.

[39] For structures with different sized atoms (Al-Co and Al-Mn-Si), a systematic change in lattice constant should be expected; but in fact we found $\rho_{\rm el} \simeq \rho_0$ in the case of $Al_{13}Co_4$ and $Al_9Co_2$, so we retained their physical lattice constants.

[40] K. Hiraga, M. Kaneko, Y. Matsuo, and S. Hashimoto, Philos. Mag. B **67**, 193 (1993).

[41] R. C. Hudd and W. H. Taylor, Acta Crystallogr. **15**, 441 (1962).

[42] A. M. B. Douglas, Acta Crystallogr. **3**, 19 (1950).

[43] J. A. Bland, Acta Crystallogr. **11**, 236 (1958).

[44] A. Kontio, E. D. Stevens, P. Coppens, R. D. Brown, A. E. Dwight, and J. M. Williams, Acta Crystallogr. B **36B**, 435 (1980).

[45] C. B. Shoemaker, D. A. Keszler, and D. P. Shoemaker, Acta Crystallogr. B **45B**, 13 (1989).

[46] M. A. Taylor, Acta Crystallogr. **12**, 393 (1959).

[47] M. Cooper and K. Robinson, Acta Crystallogr. **20**, 614 (1966).

[48] A. D. I. Nicol, Acta Crystallogr. **6**, 285 (1953).

[49] A. Kontio and P. Coppens, Acta Crystallogr. B **37B**, 433 (1981).

[50] J. G. Varlock and L. F. Mondolfo, Z. Metallkd. **66**, 605 (1975).

[51] P. Villars and L. D. Calvert, *Pearson's Handbook of Crystallographic Data for Intermetallic Phases* (American Society for Metals, Metals Park, Ohio, 1985).

[52] From these results, we might speculate that the partial occupations appearing in the crystallographic refinements of structures represent not simply thermally excited vacancies, but rather imperfect ordering of a vacancy-ordered ground state.

[53] This is a slight abuse of language: strictly/properly, an ''approximant'' has a unit cell which is a fragment of the hypothesized (ideal) infinite quasiperiodic structure with icosahedral symmetry.

[54] M. E. J. Newman, C. L. Henley, and M. Oxborrow, Philos. Mag. B **71**, 991 (1995).

[55] M. Mihalkovič and P. Mrafko, Europhys. Lett. **21**, 463 (1993).

[56] The need for high symmetry, so as to speed the relaxation, clashes with the need to represent a variety of inequivalent local patterns in the tilings. Furthermore, where *atoms* are in high-symmetry sites, the symmetry in this special case sometimes suppresses a generic trend for the atom to be unstable.

[57] Large perp fluctuations means that there are large phason strains in portions of the unit cell. In turn phason strain, crudely speaking, quantifies the deviation from average icosahedral symmetry in local regions. The importance in this in the present work is that (i) interactions which penalize perp space differences increase the stiffness against phason fluctuations, and hence promote long-range order and (ii) there is a ''phason-phonon coupling,'' i.e., the phason strain drives elastic strain which distorts the cell shapes.

[58] Variations in the relative fraction of $B$ and $E$ cells are similarly possible, but have less dramatic effects since the number of MI does not change, and since $E$ and $B$ cells are decorated in similar ways.

[59] Imagine that we had replaced the $D$ cell by an $E$ cell, attached at the same *upper* Y face. Then the atomic arrangements coincide in the upper part of the cells; in particular the two Mn($\nu$) sites on the short oblate rhombohedron ($OR_Z$) axis, in the $E$ cell, correspond to the $\gamma_{3D}$ and Mn($\nu$) sites at the upper prolate rhombohedron ($PR_D$) tip, in the $D$ cell. Since Mn works on that site in the $E$ cell, this seems to justify a possible Mn($\gamma_{3D}$) variant in the $D$ cell also.

[60] Mn($\gamma_{3D}$) is unusual for an Mn site, however, in having four other Mn in its first coordination shell. [The Mn($\delta_Y$) site would also have three Mn first neighbors]. Recall that our potentials are quite unreliable for clusters of more than two Mn in nearest-neighbor contact.

[61] We have not tested the full range of alternatives for the $\gamma_Z$ rings, in our decoration models, and there would be some technical obstacles to doing so. Any decoration must respect the symmetry of the object being decorated, and in particular the $\bar{3}$ symmetry of the $E$ cell permits only the 6/6 option for its ring of $\gamma_Z$ sites. Similarly, the other $\gamma_Z$ rings are ''bound'' to the $Z$ face, which has a single mirror plane ruling out the 5/6 but admitting the 4/6 option. Thus, the ''5/6'' variant for $\gamma_Z$ could not appear in any of our decoration rules.

[62] Note that in the 4/6 and 5/6 variants, it is *not* favorable for the $\gamma_Z$ atoms to space themselves more uniformly around the ring: the surrounding atoms on vertices of the OR force them to sit like a lattice gas on sites of the sixfold ring.

[63] As noted in paper I, the DO 6D-cut model (3/2 approximant) and the LS1.1 (or LS2.1) decorations (on tiling $T6$), are topologically equivalent except for containing (respectively) the 5/6 and the 4/6 (or 6/6) variants for the $\gamma_Z(Z_D)$ rings. After relaxing these models (with $r_{cut}=6.2$ Å), we concluded that the 5/6 ring is slightly higher in energy than the 4/6.

[64] M. Mihalkovič, M. Oxborrow, and C. L. Henley (unpublished).

[65] M. de Boissieu, C. Janot, and J.-M. Dubois, J. Phys. Condens. Matter **2**, 2499 (1990).

[66] The transition-metal network also shows great rigidity and stability in a rather different calculation on $d$-AlCo, in which atoms hopping as a lattice gas on candidate sites are simulated by Monte Carlo at an elevated temperature [M. Widom and E. Cockayne (personal communication)].

[67] C. Janot, J.-M. Dubois, M. De Boissieu, and J. Pannetier, Physica B **156&157**, 25 (1989).

[68] We have checked that rebinding the Al($\beta$) orbit decreases the rms. (The rebound sites are associated with $c$ linkages, $b$ linkages, or $D$ cell corners emanating at the MI center.)

[69] The tilings decorated in dense relaxations were *not* exactly the same tilings listed in Table II and used for loose relaxations.

[70] C. Janot, M. De Boissieu, J.-M. Dubois, and J. Pannetier, J. Phys. Condens. Matter **1**, 1029 (1989).

[71] M. Cornier-Quiquandon, A. Quivy, S. LeFebvre, E. Elkaim, G. Heger, A. Katz, and D. Gratias, Phys. Rev. B **44**, 2071 (1991).

[72] A. Katz and D. Gratias, in *Lectures on Quasicrystals*, edited by F. Hippert and D. Gratias (Les Editions de Physique, Les Ulis, France, 1994).

[73] For the smallest approximants the entire model (and hence the MI density) is virtually the same. Indeed the 2/1 cubic approximant of the DO model is topologically equivalent to the corresponding CCT approximant tiling $T5$ (in Table II) with any of the loose decorations LS$n.x$ (in the nomenclature of Sec. IV). The 3/2 DO approximant is equivalent to decoration LS1.$x$ on tiling $T6$, except that the $\gamma_Z(Z_D)$ rings are modified to the ''5/6'' variant; here $x$ codes the chemistry chosen for $\delta$ site (i.e., 6D body center).

[74] C. L. Henley and V. Elser, Philos. Mag. B **53** (3), L59 (1986).

[75] F. Nori, M. Ronchetti, and V. Elser, Phys. Rev. Lett. **61**, 2774 (1988).

[76] Such calculations have been done for Al-Co structures [M. Widom (personal communication)].

[77] The low occupation of the $\delta$ network may be encouraged by the peculiar shape of the Al-Al potential, which tends to favor vacancies in sites surrounded by Al, as explained in Appendix A.

[78] But we should be cautious in relying on refinements for the $\delta$-site occupancy: it is known that spurious sites in real-space structure can be introduced due to truncation of the wave-vector range of diffraction data used in the fit. See M. de Boissieu, C. Janot, and J.-M. Dubois, Europhys. Lett. **7**, 593 (1988), and Y. Ma, E. A. Stern, X.-O. Li, and C. Janot, Phys. Rev. B **11**, 8053 (1989).

[79] N. K. Mukhopadhyay, S. Ranganathan, and K. Chattopadhyay, Philos. Mag. Lett. **56**, 121 (1987); C. L. Henley, *ibid.* **58**, 87 (1988).

[80] M. Boudard, M. de Boissieu, and C. Janot, Europhys. Lett. **23**, 181 (1993).

[81] In Ref. 33, it is also noted that Al does not really fit in this site; they propose it is occupied preferentially by Si in $i$-AlMnSi.

[82] C. L. Henley, in *Quasicrystals*, edited by T. Fujiwara and T. Ogawa (Springer, Berlin, 1990).

[83] If so, this would reveal that the geometry underlying the Al-TM structure was not exactly the CCT, but something like a three-dimensional version of the binary tiling. That is, it would consist of a network of two inequivalent kinds of nodes, decorated with two kinds of symmetric cluster in the spirit of Burkov's Al-Co decoration.

[84] The representation of structural energy by effective Hamiltonians has been applied profitably in other contexts, e.g., parametrizing the energetics of stacking fault sequences in long-period superlattices using the ANNNI model.

[85] The validity of the results in Table XII is limited by the range of models we considered. For example, $V_E'$ is unphysically large for all of our CCT models, since the high symmetry of the $E$ cell condemns it to carry an overpacked 6/6 ring of $\gamma_Z$(Al) (see Sec. IV C 1), whereas the real alloy surely lowers its energy by admitting one or two vacancies randomly on every such ring.

[86] If the tile Hamiltonian is fitted using the *unrelaxed* energies, then (for $r_{\rm cut}=6.2$ Å) the errors corresponding to Table XIII are essentially zero. That means the tile-tile terms, reflected in Table XIII, are overwhelmingly mediated elastically, rather than direct interactions due to the second well.

[87] When the CCT network itself is distorted, these displacements can be considered the result of phonon-phason coupling.

[88] M. E. J. Newman and C. L. Henley, Phys. Rev. B **52**, 6386 (1995).

[89] C. L. Henley, Phys. Rev. B **34**, 797 (1986).

[90] M. Mihalkovič and P. Mrafko, Phys. Rev. B **49**, 100 (1994).

[91] See G. Trambly de Laissardiere and T. Fujiwara, Phys. Rev. B **50**, 9843 (1994). They computed electronic structure of *d*-AlCuCo initially using a pseudobinary model which mixed Co and Cu, but were forced to modify it by a particular assignment of Cu and Co atoms, in order to obtain a sensible electronic structure. In some sense, this computation has buried in it the same kind of information that is approximated by pair potentials for a ternary.

[92] Currently work is in progress on potentials for AlPdMn [M. Windisch and J. Hafner (personal communication)].

[93] Indeed, since we did not attempt to optimize the residuals in Table XIII, it is likely we could substantially reduce them even for the *i*-AlMn case.

[94] G. Coddens, C. Soustelle, R. Bellissent, and Y. Calvayrac, Europhys. Lett. **23**, 33 (1993).

[95] The independent process of ''phason-assisted diffusion'' involves clusters dissolving and the reforming nearby. See P. A. Kalugin and A. Katz, Europhys. Lett. **21**, 921 (1993); M. V. Jarić and E. S. Sorensen, Phys. Rev. Lett. 73, 2464 (1994); and F. Gähler and J. Roth, in *Aperiodic Crystals '94* (Ref. 6), p. 183.

[96] However, a different scenario seems to be observed in *d*-AlCo: only Co atoms stay fixed, while all Al sites (including those in the ''pentagonal bipyramid'' clusters analogous to MI's) seem to show random occupations at high temperatures [M. Widom (personal communication)]; See E. Cockayne, M. Widom, P. Launois, M. Fettweis, and F. Dénoyer, in *Aperiodic '94* (Ref. 6), p. 578.